https://doi.org/10.5194/acp-2021-797
Preprint. Discussion started: 26 October 2021

Atmospheric Chemistry and Physics Discussions

Characterizations of Europe's integrated water vapor and assessments of atmospheric reanalyses using more than two decades of ground-based GPS

Peng Yuan[1], Roeland Van Malderen[2], Xungang Yin[3], Hannes Vogelmann[4], Joseph Awange[5], Bernhard Heck[1], Hansjörg Kutterer[1]

[1]Geodetic Institute, Karlsruhe Institute of Technology, Karlsruhe, 76131, Germany
[2]KMI-IRM, Royal Meteorological Institute of Belgium, Brussels, B-1180, Belgium
[3]Riverside Technology Inc, Asheville, NC 28801, USA
[4]Karlsruhe Institute of Technology, IMK-IFU, Garmisch-Partenkirchen, 82467, Germany
[5]Curtin University, School of Earth and Planetary Sciences, Perth, WA 6845, Australia

Correspondence to: Peng Yuan (peng.yuan@kit.edu)

Abstract. Ground-based Global Positioning System (GPS) has been extensively used to retrieve Integrated Water Vapor (IWV) and has been adopted as a unique tool for the assessments of atmospheric reanalyses. In this study, we investigated the multi-temporal-scale variabilities and trends of IWV over Europe by using IWV time series from 108 GPS stations for more than two decades (1994-2018). We then adopted the GPS IWV as a reference to assess six commonly-used atmospheric reanalyses, namely CFSR, ERA5, ERA-Interim, JRA55, MERRA2, and NCEP2. The GPS results show that the diurnal cycles peak within 16:00-24:00 local time with peak-to-peak amplitudes accounting for 2%-18% of the daily mean. The diurnal 1-hourly anomalies can be much more intensive with a range of −100% to 200%. The annual cycles peak in July and August with maximum values of 17-32 kg m^{-2}. The interannual variations of IWV over Europe are found to be mainly linked to the North Atlantic Oscillation (NAO) and the East Atlantic (EA) patterns. The IWV continues to increase over Europe during the last two decades at 0-0.4 kg m^{-2} $decade^{-1}$ in the north and 0.4-1 kg m^{-2} $decade^{-1}$ in the south. Regarding the assessments of the reanalyses, the intercomparisons with respect to GPS reveal a general superiority of the newly-released ERA5 IWV product. For instance, ERA5 only has a slight wet bias with a median value of 1%, whereas the median bias for MERRA2 is 4%. ERA5, MERRA2, and NCEP2 are the best, second best, and worst performers respectively in modelling the variability of daily IWV time series, with standard deviations of daily IWV differences against GPS by 0.5-1.6, 0.7-2.3, and 1.2-3.0 kg m^{-2}, respectively. Moreover, the daily GPS IWV time series is best correlated with the ERA5 IWV with a median Pearson correlation coefficient of 0.996, whereas the second strongest and weakest median correlations are observed in MERRA2 and NCEP2 with values of 0.991 and 0.971, respectively. Furthermore, the correlations between the IWV trends from the reanalyses and GPS are strongest for ERA5 (0.82), a bit weaker for MERRA2 (0.72), and weakest for NCEP2 (0.52).

1 Introduction

Water vapor serves as an important medium of moisture and latent heat transfer in the Earth's atmosphere on the one hand, while on the other hand, it is the most important gaseous source of infrared opacity in the atmosphere and the largest

https://doi.org/10.5194/acp-2021-797
Preprint. Discussion started: 26 October 2021

Atmospheric Chemistry and Physics Discussions

contributor to the natural greenhouse effect (Kiehl and Trenberth, 1997). It plays a key role in water and energy cycle (e.g, Trenberth and Fasullo, 2013), climate change (e.g, Schneider et al., 2010), and various weather and climate processes (e.g, Haar et al., 2012), and is crucial for the understanding of many extreme events, such as atmospheric rivers (e.g, Zhu and Newell, 1994), hurricanes (e.g, Ejigu et al., 2021), floods (e.g, Turato et al., 2004), and droughts and monsoons (e.g., Jiang et al., 2017; Fadnavis et al., 2021). Due to its large spatiotemporal variability, its high-accuracy quantification remains a challenge (Vogelmann et al., 2015).

Characterizing the multiple spatiotemporal scale variabilities and long-term trends of water vapor is of great importance for Europe, which is like a peninsula of the Eurasian landmass surrounded mainly by the Arctic Ocean, Atlantic Ocean, and Mediterranean Sea, to the north, west, and south, respectively. Owing to the moisture from the oceans carried by the prevailing westerlies, most of Western Europe has an oceanic climate with mild, wet, and turbulent weather in winter. In contrast, Southern Europe is characterized by a well-known dry-summer Mediterranean climate. Europe is generally vulnerable to the extreme events associated with abnormal water vapor transport and very sensitive to climate change (Field and Barros, 2014; Lavers et al., 2016), and has been the fastest warming up continent in recent decades (e.g., Copernicus, 2019). Since 1 K rise in temperature could contribute to a 7% increase of water vapor holding capacity as implied by the Clausius–Clapeyron equation (Trenberth et al. 2003), Europe's water vapor amount is noticeably increasing (Yuan et al., 2021). The increasing water vapor content has a stronger greenhouse effect, leading to a higher temperature, and thus forms a positive feedback loop (Held and Soden, 2000). The warmer and moister climate impacts all weather events and aggravates the risks of extreme events (Trenberth, 2012).

Atmospheric water vapor content can be expressed by using Integrated Water Vapor (IWV), which is defined as the total amount of water vapor present in a vertical atmospheric column from the Earth's surface to the top of the atmosphere in unit of kg m^{-2} (Jones et al., 2020). The IWV is also known as the Total Column Water Vapor (TCWV) or Precipitable Water Vapor (PWV). At present, numerous techniques have been developed to measure water vapor, such as balloon-borne radiosondes (e.g., Durre et al., 2009; Kunz et al., 2013; Müller et al., 2016), aircraft measurements (e.g., Tilmes et al., 2010; Kunz et al., 2014; Krämer et al., 2020), satellite observations (e.g., Grossi et al., 2015), and ground-based methods (e.g., Kämpfer 2012; Vogelmann et al., 2015). Global Navigation Satellite System (GNSS), represented by the USA's NAVSTAR Global Positioning System (GPS), has been exploited for water vapor retrieval by using its ground-based measurements (e.g., Bevis et al., 1992) or space-based radio occultation (e.g., Kursinski et al., 1995) since the 1990s. Though accurate vertical distribution of water vapor in the upper troposphere can be obtained by the GPS radio occultation (e.g., Randel and Wu, 2005; Randel et al., 2007), its accuracy is limited in the lower troposphere (e.g., Ao et al., 2003; Awange 2012,2018) where the water vapor is most abundant. On the contrary, the ground-based GPS has proven to be an effective technique for IWV retrieval with advantages of high accuracy, high temporal resolution, and all-weather condition availability (Jones et al., 2020). The ground-based GPS has been utilized for IWV measurement in numerous global (e.g., Wang and Zhang, 2009; Vey et al., 2010; Chen and Liu, 2016) as well as regional (e.g., Bernet et al., 2020; Ejigu et al., 2021; Huang et al., 2021) studies. In addition, there have been nearly three decades of continuous GPS measurements with increasingly densified

https://doi.org/10.5194/acp-2021-797
Preprint. Discussion started: 26 October 2021

Atmospheric Chemistry and Physics Discussions

networks in Europe, such as the European Reference Frame (EUREF) Permanent Global Navigation Satellite System (GNSS) Network (EPN; Bruyninx et al., 2012). Given these benefits, ground-based GPS offers a unique tool to investigate the multiple spatiotemporal scale variabilities of IWV over Europe, especially the associated extreme weather and climate events (Bonafoni et al., 2019). The homogeneously reprocessed long-term time series of GPS IWV is also quite beneficial to climate change studies (e.g., Van Malderen et al., 2020). GPS has increasingly been adopted to investigate various temporal features of Europe's IWV in many studies, such as diurnal cycle (e.g., Wang et al., 2009; Diedrich et al., 2016; Steinke et al., 2019), seasonal variations (e.g., Parracho et al., 2018), interannual variations (e.g., Khutorova et al., 2018), and trends (e.g., Nilsson and Elgered 2008, Ning et al., 2016, Wang et al., 2016). However, the multi-temporal-scale variabilities and trends of Europe's IWV have rarely been comprehensively studied using GPS.

Atmospheric reanalyses have been extensively adopted as the data source of IWV acquisition for the last several decades, owing to the benefits of regional/global coverage, consistent spatiotemporal resolution, and the availability of many other meteorological variables. However, their products may still be subject to large uncertainty. On the one hand, this is due to the fact that the reanalyses from different providers and different versions are inconsistent in the input data, assimilation schemes, besides using different physical schemes and representations. For example, the newly released fifth generation global reanalysis from ECMWF (ERA5; Hersbach et al., 2020) has assimilated more datasets and instruments, which were not ingested in its predecessor ERA-Interim (ERAI; Dee et al., 2011). The assimilation system of ERA5 is also more advanced. On the other hand, systematic and random errors in the input data are unavoidable. For instance, the Integrated Global Radiosonde Archive (IGRA, Durre et al., 2018) provides a long record of relative humidity observations for the assimilation of reanalysis, but long-term radiosonde humidity measurements are very sensitive to changes in instrumentation and measuring practice (McCarthy et al., 2009, Dai et al., 2011). Therefore, assessments of the reanalyses' water vapor products are indispensable for the accurate understanding and interpretations of Europe's weather and climate processes. The performances of various reanalyses' IWV products in Europe have been assessed by many regional/global studies using ground-based GPS data, as the GPS observations are not operationally assimilated by reanalyses (Hagemann et al., 2003; Bock et al., 2005; Heise et al., 2009; Vey et al., 2010; Alshawaf et al., 2018; Parracho et al., 2018; Wang et al., 2020; Yuan et al., 2021). However, it is still quite hard to draw consistent conclusions on the performances of different reanalyses from these studies, as they are different in many aspects, such as the numbers and locations of the GPS stations, period of observations, data processing strategies, and performance metrics. A consistent assessment of various reanalyses by using homogeneously reprocessed long-term time series of GPS IWV as reference in Europe is still lacking. In addition, few studies have focused on the performance of the latest ERA5 in reproducing the temporal features of Europe's IWV so far.

In this paper, we focus on characterizing the multi-temporal-scale variabilities and trends of Europe's IWV -using more than two decades of GPS IWV, and then we assess the performances of six reanalyses' IWV products over Europe. The paper is organized as follows: In section 2, we describe the GPS and reanalyses datasets, IWV calculation methods, and consistency evaluation metrics. Section 3 assesses the consistency in daily time series and representativeness differences, while the diurnal variations and the associated diurnal cycle, annual variations and interannual anomaly, and long-term

https://doi.org/10.5194/acp-2021-797
Preprint. Discussion started: 26 October 2021


Atmospheric Chemistry and Physics Discussions

trends of Europe's IWV are investigated using GPS in sections 4, 5, and 6, respectively. The performances of the reanalyses are also assessed accordingly, and the main findings are summarized in section 7.

2 Data and methods

2.1 GPS data

To characterize the IWV over Europe and assess the reanalyses, 1-hourly GPS IWV retrievals obtained from 108 stations are used (Fig. 1). Most of GPS stations are from the EPN network. The GPS observations are from January 1994 to December 2018 with an average time length of 21 years and an average integration rate of 95% (Table S1). The IWV retrievals were estimated with GPS Zenith Total Delay (ZTD) provided by the Nevada Geodetic Laboratory (NGL, Blewitt et al. 2018). The NGL processes the GPS data using the newly improved GipsyX v1.0 software in PPP mode (Bertiger et al., 2020). Reprocessed orbits and clocks from Jet Propulsion Laboratory (JPL) Repro 3 were used together with the 2014 International GNSS Service (IGS) reference frame (IGS14; Rebischung and Schmid, 2016). The observations were weighted based on elevation whose cutoff angle was set to 7°. The first order effect of the ionosphere was removed by employing ionosphere-free combinations of the GPS observations. The second order effect was corrected with International Geomagnetic Reference Field 12 (IGRF12; Thébault et al., 2015) and JPL's ionosphere maps. As for the modelling of tropospheric delay, the Vienna Mapping Function 1 (VMF1; Boehm et al., 2006) and its associated *a priori* Zenith Hydrostatic Delay (ZHD) were adopted.

2.2 Reanalysis data

The IWV derived from six commonly-used global atmospheric reanalyses, namely, the newly released fifth generation global reanalysis (ERA5) and its predecessor ERA-interim (ERAI) from ECMWF, the Japanese 55-year Reanalysis (JRA55) from Japan Meteorological Agency (JMA), the Modern-Era Retrospective Analysis for Research and Applications, version 2 (MERRA2) from NASA Global Modeling and Assimilation Office (GMAO), and the Climate Forecast System Reanalysis (CFSR) and NCEP-DOE AMIP-II Reanalysis (NCEP2) from National Centers for Environmental Prediction (NCEP) are analyzed. The features of the reanalyses are summarized in Table 1. It is worth noting that JRA55 only provides humidity information at 27 pressure levels from 1000 to 100 hPa, though it has 37 levels in total. These six reanalyses are selected as their IWV products cover the period of the ground-based GPS data available since 1994. Despite ERAI having been decommissioned and superseded by ERA5 in August 2019, we still include it for the purpose of evaluating the progress of its successor ERA5. We therefore restricted the time range of all data records to a common period from 1994 to 2018.

2.3 Teleconnection indices

Previous studies have demonstrated that the variations of atmospheric water vapor are linked to various teleconnection patterns (e.g., Wang et al., 2018; Thomas et al., 2021). In this study, teleconnections between the extreme IWV anomalies in

https://doi.org/10.5194/acp-2021-797
Preprint. Discussion started: 26 October 2021

Atmospheric Chemistry and Physics Discussions

Europe and eight indices are evaluated, including (1) North Atlantic Oscillation (NAO; Barnston and Livezey, 1987), (2) East Atlantic pattern(EA; Barnston and Livezey, 1987), (3) Arctic Oscillation (AO; Thompson and Wallace, 1998), (4) Scandinavia pattern (SCA; Comas-Bru and McDermott 2014), (5) Western Mediterranean Oscillation (WeMO; Martin-Vide and Lopez-Bustins, 2006), (6) Niño 3.4 index (Trenberth, 1997), (7) Northern Oscillation Index (NOI; Schwing et al., 2002), and (8) Quasi-Biennial Oscillation (QBO; Baldwin et al., 2001). The well-known NAO, characterized by a meridional dipole in atmospheric pressure between the Azores High and Icelandic Low, is a prominent mode of winter climate variability over Europe (Hurrell 1995; Comas-Bru and McDermott., 2014). It exerts a dominant influence on air temperature, water vapor, precipitation, and wind patterns over the Atlantic/European sector, especially during the boreal winter (Trigo et al., 2002). The EA pattern is known to be the second leading mode of the climate variability over the Atlantic/European sector (Barnston and Livezey, 1987) and it can modulate the structure and climate impact of the NAO (Moore and Renfrew, 2012). For information on the other indices, readers are referred to the relevant references.

2.4 IWV retrievals

The Zenith Total Delay (ZTD) estimates derived from GPS data processing can be converted into IWV, the total amount of water vapor present in a vertical atmospheric column from the Earth's surface to the top of the atmosphere in unit kg m^{-2}, using the following equation (Bevis et al., 1992):

$$\mathrm{IWV} = \frac{10^6}{R_V \cdot [k_2' + k_3/T_m]} \cdot (\mathrm{ZTD} - \mathrm{ZHD}), \quad (1)$$

where R_V denotes the gas constant for water vapor, k_2' and k_3 are atmospheric refractivity constants (Bevis et al., 1994), and T_m denotes the weighted mean temperature. The ZHD was modelled as follows (Saastamoinen, 1972; Davis et al., 1985):

$$\mathrm{ZHD} = 2.2768 \frac{P_s}{1 - 2.66 \times 10^{-3} \cdot \cos(2\varphi_s) - 2.8 \times 10^{-7} H_s}, \quad (2)$$

where P_s denotes the pressure at the GPS station with a latitude of φ_s and height of H_s.The P_s and T_m are computed by using the ERA5 pressure level product (see Yuan et al., 2021 and references therein). The ERA5 is selected as it can provide 1-hourly product without temporal interpolation.

IWVs at the GPS stations are also calculated from the six reanalyses. In this calculation, the pressure level products of the reanalyses are used rather than their surface level IWV products, though it requires a heavier workload. This is because the GPS station and its nearby reanalysis surface grids are usually related to different heights. Vertical IWV adjustment is therefore usually required for the intercomparison between the IWV estimates from GPS and reanalyses Compared to the reanalyses' surface level products, their pressure level products allow for a better characterization of the vertical distribution of water vapor and tends to minimize the errors of the vertical adjustment (Parracho et al., 2018).

The scheme of the calculation is illustrated in Fig. 2. Assume a GPS station G with a height of H_s located between two adjacent reanalysis pressure levels ($\boldsymbol{P_j}$ and $\boldsymbol{P_{j+1}}$). We first determined its eight surrounding reanalysis grid nodes at these pressure levels (N_j^i and N_{j+1}^i, i=1, 2, 3, and 4) and four auxiliary points (A_i). The auxiliary points are located at the GPS

https://doi.org/10.5194/acp-2021-797
Preprint. Discussion started: 26 October 2021

Atmospheric Chemistry and Physics Discussions

station height whereas their horizontal locations are identical to the associated reanalysis nodes. We then calculate the related meteorological variables at each auxiliary point. Exponential and linear interpolations are employed for the vertical corrections of pressure and temperature, respectively. If the auxiliary point is lower than the lowest pressure level (e.g., 1000 hPa), an extrapolation of these variables is conducted. For details of the vertical inter- /extrapolation, readers are referred to Schüler (2001) and Wang et al. (2005). Next, we calculate the IWV at each auxiliary point by using a vertical integration:

$$\mathrm{IWV}_i = \int \frac{q}{g} dP, \quad (3)$$

where q and g are specific humidity and gravitational acceleration profiles from H_s to the reanalysis top level, respectively.

Finally, we estimate the IWV at the GPS station using a horizontal interpolation with an inverse distance weighting algorithm (Jade and Vijayan, 2008).

Representativeness differences arise in the comparison of the IWV derived by the ground-based GPS and reanalyses (Bock and Parracho, 2019). This is because local variations of IWV measured by the GPS might fail to be resolved by the reanalyses due to their coarse horizontal resolution. The representativeness differences can be evaluated statistically as proposed by Bock and Parracho (2019):

$$\delta_{\max} = max\left(\left|\mathrm{IWV}_i - \mathrm{IWV}_k\right|\right),\ i,k = 1,2,3,4,\ i \neq k, \quad (4)$$

where IWV_i and IWV_k are the IWV values of the horizontal auxiliary points A_i and A_k, respectively (Fig. 2). Bock and Parracho (2019) found that the $\delta_{\max}$ was correlated with the standard deviation of the IWV differences between GPS and ERAI (σ_Δ), and thus concluded that the representativeness differences between the IWV from GPS and ERAI contributed to their discrepancies. Here, we extend their work by estimating and comparing the representativeness statistics of the six reanalyses with various spatial resolutions (Table 1).

2.5 Pre-processing

The 1-, 3-, and 6-hourly IWV time series are screened by using a robust outlier detection method as follows (Yuan et al., 2021). For each data point, the data within a 30-day window centered at this point are extracted. The 25th percentile (Q1), 75th percentile (Q3), and interquartile range (IQR) of the subsequent time series are then calculated. Finally, the data point is identified as an outlier if it is outside the range of $[\mathrm{Q1} - 1.5 \times \mathrm{IQR}, \mathrm{Q3} + 1.5 \times \mathrm{IQR}]$. The IQR threshold and the 30-day sliding window are adopted as they allow for a good robustness and a proper accommodation for the natural variability of IWV. On average, about 1% data were filtered out by the data screening.

The GPS IWV time series may have breaks due to changes in GPS data processing strategies and station-related changes like hardware changes or changes in the electromagnetic environment (Van Malderen et al., 2020 and references therein). Changes in GPS data processing strategy are avoided in this study by using the homogeneously reprocessed GPS ZTD product. Moreover, the GPS IWV time series are homogenized as described in Yuan et al. (2021). The difference in time series between GPS and ERA5 IWV are then calculated, so that most of the natural IWV variabilities are removed and the small breaks are easily distinguishable. The associated GPS height time series and station log files are also inspected to

https://doi.org/10.5194/acp-2021-797
Preprint. Discussion started: 26 October 2021

Atmospheric Chemistry and Physics Discussions

195 find out suspicious epochs of device changes. The significances of the breaks are tested at 95% confidence level with the specific optimal noise model of each IWV difference time series. The IWV time series from reanalyses may also have breaks (e.g., Ning et al., 2016, Schröder et al, 2016), and thus we compared them with the homogenized GPS IWV time series. Nevertheless, no obvious breaks were found in the reanalyses time series.

In this study, the performances of reanalyses IWV products in daily time series, 1-hourly diurnal cycle and variations, 200 1-monthly annual cycle and interannual variations, and trends are evaluated. As the temporal resolutions of the datasets are different, temporal interpolation and aggregation are conducted. For the investigation of diurnal cycle and variations, the 3- and 6-hourly IWVs are linearly interpolated into 1-hourly time series. To obtain daily mean IWVs, the 1-, 3-, and 6-hourly IWV time series are aggregated if they have at least 12, 4, and 2 data points in a day, respectively. The daily mean IWVs are further aggregated into monthly mean IWVs if there are no less than 15 data points in a month.

205 2.6 Metrics for consistency evaluation

To evaluate the performances of the reanalyses in reproducing IWV, Kling-Gupta Efficiency (KGE) is employed as a metric. The KGE is a composite index introduced by Gupta et al. (2009) and modified by Kling et al. (2012). It takes bias, variability, and correlation into account in the equation below:

$$\mathrm{KGE} = 1 - \sqrt{(\beta - 1)^2 + (\gamma - 1)^2 + (r - 1)^2}, \quad (5)$$

210 with

$$\beta = \frac{\mu_R}{\mu_G}, \quad (6)$$

$$\gamma = \frac{CV_R}{CV_G} = \frac{\sigma_R/\mu_R}{\sigma_G/\mu_G}, \quad (7)$$

and μ_R, σ_R, and CV_R are the mean value, standard deviation, and coefficient of variation of the reanalysis IWV time series, respectively. The μ_G, σ_G, and CV_G are the corresponding parameters for GPS. The β and γ indicate the consistencies in the 215 mean and variability, respectively. The r indicates the Pearson correlation coefficient between the GPS and reanalyses time series. With perfect consistencies in mean, variability, and correlation, the β, γ, and r are identical to 1, respectively. From Eq. (5), it follows that a larger KGE score indicates a better consistency. Ideally, the KGE metric reaches its maximum of 1.

3 Assessments of daily time series

3.1 Representativeness differences

220 Figure 3 compares the standard deviations of daily IWV difference (σ_Δ) and the representativeness statistic ($\delta_{\max}$) for the six reanalyses, respectively. The first point to note is that the σ_Δ and $\delta_{\max}$ are strongly correlated for all the reanalyses, with values from 0.74 for NCEP2 to 0.91 for ERA5. The result is in line with Bock and Parracho (2019), who compared ERAI to a global GPS network. Figure 3 indicates that the representativeness differences contribute to the discrepancies

https://doi.org/10.5194/acp-2021-797
Preprint. Discussion started: 26 October 2021


Atmospheric Chemistry and Physics Discussions

between the reanalyses and GPS. Moreover, ERA5 is characterized by the lowest σ_Δ and δ_{max}, with values of 0.5-1.6 and 0.2-2.1 kg m^{-2}, respectively. In contrast, NCEP2 has the largest σ_Δ and δ_{max}, with values of 1.2-3.0 and 1.9-5.2 kg m^{-2}, respectively. The difference could be due to the fact that the spatiotemporal resolution of ERA5 is much higher than NCEP2 as indicated in Table 1. This result indicates that ERA5, with improved spatiotemporal resolution and data assimilation, is capable of reducing the discrepancy and representativeness difference with respect to GPS.

3.2 Assessments using KGE

Figure 4 shows the geographical distributions of the ratio of mean β, the ratio of coefficient of variation γ, the correlation r, and the synthetic KGE metric for the six reanalyses by taking the daily GPS IWV time series as references. Moreover, the statistics of these scores are displayed in Fig. 5 with box-and-whisker plots. From the first column of Fig. 4 and Fig 5a we can see that the β scores are slightly larger than 1 for all the reanalyses except JRA55, indicating a general wet bias. For example, MERRA2 has the largest median β with a value of 1.04, indicating a general wet bias of 4%. In contrast, JRA55 scores a median β of 0.99 (Fig. 5a), indicating a slight dry bias of 1%. These results are in agreement with Schröder et al. (2018), who reported that CFSR, ERAI, and MERRA2 are too moist over Europe compared to the ensemble mean of various satellite and reanalysis IWV records, whereas JRA55 has negligible bias there. Analyzing the reasons of the biases is of potential interest; however, it would go beyond the scope of this paper.

Regarding the consistency in variability, most of the γ scores are less than 1, with the associated median values ranging between 0.96 and 0.98 (Fig. 5b). The results indicate a good reproduction of daily IWV variability by the reanalyses, albeit with a slight underestimation. The correlations are also pretty good with median values larger than 0.97 (Fig. 5c). However, the scores in variability and correlation are lower for the coastal stations, as shown in the second and third columns of Fig. 4, respectively. In particular, the γ and r of NCEP2 are less than 0.96 for some coastal stations located at Western and Southern Europe. This could be explained by the representativeness differences that impact the IWV variability. For a coastal GPS station with an on-site measurement of IWV, a part of its associated four reanalysis grid nodes may be located over the sea whereas others over land. As a consequence, the representativeness difference for such a coastal site is more severe than inland stations surrounded with flat terrain due to land-sea thermal contrast (Drobinski et al., 2018).

Figure 5d compares the overall consistency in daily IWV evaluated using KGE. It can be seen that ERA5 is characterized by the largest median KGE (0.97). The result reveals the superiority of ERA5 over the other reanalyses. Moreover, comparing β, γ, and r (Fig. 5a-c) shows that r tends to contribute the least to the overall inconsistency, indicating that improving the consistencies in mean values and variabilities are more important for the daily IWV time series.

https://doi.org/10.5194/acp-2021-797
Preprint. Discussion started: 26 October 2021

Atmospheric Chemistry and Physics Discussions

4 Assessments of diurnal variations

Despite the atmospheric water vapor being quite unstable, it is characterized by a diurnal cycle (Dai et al., 2002). In this section, the diurnal variations of IWV are investigated in two aspects: diurnal cycle and diurnal anomaly. The diurnal anomaly is calculated as follows (Diedrich et al., 2016; Steinke et al., 2019):

$$\mathrm{IWV}_{DA} = \frac{\mathrm{IWV} - \overline{\mathrm{IWV}}}{\overline{\mathrm{IWV}}} \times 100\%, \quad (8)$$

where IWV is the 1-hourly IWV time series in one day and $\overline{\mathrm{IWV}}$ is the associated daily mean.

Each station's diurnal cycle is computed by averaging its diurnal anomalies for each season separately and for the entire year. We analyzed the amplitude and phases of each station's diurnal cycle. Note that, the amplitude is here defined as the difference between the maximum and minimum, i.e., the peak-to-peak amplitude. Moreover, the time of each station's diurnal variation is converted into the Local Time (LT).

4.1 Diurnal cycle

Starting with the annual-averaged peak-to-peak amplitudes of the GPS IWV's diurnal cycle in Fig. 6e, it can be first noted that the amplitudes tend to increase equatorward, with values ranging from 2% to 18%. This finding is in line with the amplitude of the IWV itself, although we consider relative amplitudes here. However, lower latitude stations also experience higher temperature contrasts over a day than higher latitude stations (Sharifnezhadazizi et al., 2019), and the IWV diurnal variability is mainly governed by the temperature diurnal variability (see Wang et al., 2016). Moreover, Fig. 7a shows that the diurnal amplitudes of GPS IWV are well correlated with station heights ($r = 0.7$). Diedrich et al. (2016) also reported the height dependence in a global analysis and attributed it to orographic circulation which enhances the temperature difference between day and night at higher altitude stations. Similar geographical patterns arise for the seasonal-averaged amplitudes (Fig. 6a-d), with identical explanations as for the overall average. An obvious feature is that the amplitudes in spring (MAM) and summer (JJA) are generally larger than those in autumn (SON) and winter (DJF), as also noted by Diedrich et al. (2016) and Steinke et al. (2019). Not only the season-dependent diurnal temperature variability plays a role in explaining this feature, but other factors also have an impact as well (Dai et al., 2002). For instance, evapotranspiration, another primary cause of the diurnal cycle of IWV, is lowest in winter (DJF) due to least transpiration of vegetation.

Concerning the phase of the IWV diurnal cycle, the GPS measurements show that most of the IWV cycles reach their minima between 5:00-12:00 LT and then peak around 16:00-24:00 LT (Fig. 6f-o). The minimum and maximum values of the yearly-averaged diurnal cycles occur around 8:00 and 19:00 LT, respectively. The result could be explained by the fact that solar insolation during the day enhances evapotranspiration and accumulates water vapor until sunset.

All the reanalyses successfully reproduce the IWV's diurnal cycle as shown in Fig. 8a-c. However, MERRA2 only scores a median KGE value of 0.62, lower than the scores of CFSR, ERAI, and JRA55 (0.71-0.75) which have a coarser original temporal resolution (6-hourly versus 3-hourly). The poor performance of MERRA2 is mostly due to its overestimation of the variability of diurnal cycle (Fig. 8a). A similar overestimation of diurnal amplitude was reported by

https://doi.org/10.5194/acp-2021-797
Preprint. Discussion started: 26 October 2021

Atmospheric Chemistry and Physics Discussions

Wang et al. (2017) in an inter-comparison of GPS and MERRA (the ancestor of MERRA2) in the southern Tibetan Plateau. In that work, the authors suggested that it could be due to an exaggerated land evaporation in MERRA (Mueller and Seneviratne, 2014), which might also exist in MERRA2 over Europe. In contrast, ERA5 reproduces the best variability (median γ=0.98). However, it only scores a median KGE of 0.72, which is at the same level of CFSR, ERAI, and JRA55. This is mainly due to its weaker correlation (Fig. 8b). Therefore, though ERA5 and MERRA2 have higher temporal resolutions than the others, future work is certainly required to improve their capabilities in reproducing the phase and amplitude of diurnal cycles of IWV, respectively.

4.2 Diurnal anomalies

Diurnal anomaly represents high-frequency variations of IWV, associated with weather phenomena like heavy rainfall. Figure 9 compares the diurnal anomalies derived from reanalyses with respect to GPS. To be consistent with the temporal resolution of GPS and ERA5, the diurnal anomalies of the other reanalyses are linearly interpolated into 1-h time series. It is observed that the anomalies roughly range from −100% to 200% of the associated daily mean IWV, indicating that the diurnal variations of IWV are much stronger than the diurnal cycles. It can also be seen that the range of GPS diurnal anomalies is larger in winter than in summer, suggesting a more intensive relative variability compared to the associated daily mean IWV. It could be due to the fact that the daily mean IWV is much lower in winter than in summer.

Figure 8d-f shows the KGE scores of the reanalyses in reproducing diurnal anomaly of IWV. It can be seen that the median KGE scores of ERA5 and MERRA2 are 0.90 and 0.77, respectively. Their scores are much better than the other four reanalyses with median scores between 0.39 and 0.58. This is not surprising as ERA5 and MERRA2 have the highest initial temporal resolution (Table 1). Therefore, ERA5 is recommended in studies of high-frequency IWV variations.

5 Assessments of annual and inter-annual variations

5.1 Annual cycle

We analyzed the annual and inter-annual variations of IWV using monthly mean time series. The annual GPS IWV cycle, as a function of latitude, is shown in Fig. 10a. The annual IWV cycles reach their maxima mostly in July and August, with peak values from 17 to 32 kg m^{-2}. In contrast, the minima of the annual cycles are noted in January and February, with values from 4 to 17 kg m^{-2}. The results are consistent with those of Wypych et al. (2018). The maximum and minimum values of the annual cycles are generally increasing with decreasing latitude (Fig. 10a) and decreasing altitude (not shown). Figure 10b-g presents the differences between the annual cycle of IWV estimated by the reanalyses with respect to GPS. It can be seen that ERA5 has the least differences. Indeed, the quantitative evaluation shows that ERA5 obtains the highest median KGE score having a value of 0.97 (Fig. 5h). Moreover, the median KGE scores of the other reanalyses are also rather good (>0.94). The results indicate that all the reanalyses reproduce the annual cycle of IWV quite well, with ERA5 slightly outperforming the other reanalyses.

https://doi.org/10.5194/acp-2021-797
Preprint. Discussion started: 26 October 2021

Atmospheric Chemistry and Physics Discussions

315 **5.2 Interannual variations and teleconnections**

The interannual variations of IWV are investigated by using its monthly relative anomalies. The relative anomaly of a month is calculated as the ratio between the IWV change of that month relative to the multiyear mean value of that month. The monthly relative anomaly time series of GPS IWV are presented in Fig. 11a with decreasing latitudes. It could be noted that the majority of robust IWV anomalies occurs in winter (DJF), with amplitudes as large as 50%. Those winter IWV 320 anomalies are found to be linked to NAO. with a pattern that the NAO index and IWV anomalies are strongly positively correlated in Northern Europe and slightly negatively correlated in Southern Europe (Fig. 11d). This finding points to a wetter (drier) weather condition in Northern Europe and a drier (wetter) condition in Southern Europe when NAO is in its positive (negative) phase. The spatial pattern is in line with Trigo et al. (2002) and can be explained by the fact that during positive NAO phase, the path of moisture transport turns towards a more northeast orientation over the North Atlantic than 325 usual, and thus results in enhanced (reduced) moisture transport over Northern (Southern) Europe (Hurrell. 1995). The modulation of NAO on the IWV over Europe is also consistent with its influence on temperature and precipitation. Previous studies have demonstrated that a positive NAO phase tends to be accompanied by reinforced westerly winds over the North Atlantic, which is conducive to above-average temperature and precipitation over Northern Europe as well as below-average precipitation over Southern Europe (e.g., Hurrell 1995). During negative NAO phases, opposite patterns of temperature and 330 precipitation anomalies are expected.

In addition, the IWV anomalies in winter are also significantly correlated to the EA pattern (Fig. 11e). The positive correlation between EA and IWV over Europe indicates a wetter (drier) condition with positive (negative) EA phase. This teleconnection could be attributed to the influence of EA on atmospheric circulation. The winter positive (negative) EA phase indicates a dominating zonal (meridional) circulation (Mikhailova and Yurovsky et al., 2016). Hence, EA can 335 modulate heat and moisture transport. A positive EA index in winter indicates a higher likelihood of higher-than-usual temperature over Europe, enhanced precipitation in Northern Europe, and precipitation deficiency in Southern Europe. By contrast, a negative EA index is likely to result in opposite influences on temperature and precipitation.

As the winter atmospheric circulation over the Atlantic/European sector can be mostly represented by NAO and EA, the joint effects of NAO and EA on the winter IWV anomalies are investigated with four cases, namely (i) both NAO and 340 EA are positive, (ii) NAO is positive whereas EA is negative, (iii) NAO is negative whereas EA is positive, and (iv), both NAO and EA are negative:

(i) Both NAO and EA are positive

The winters of 2013/2014 and 2015/2016 are characterized by pronounced positive IWV anomalies (Fig. 11a). The results could be explained by the positive NAO and EA indices anomalies (Fig. 11b-c), which indicate a general milder and wetter 345 condition over Europe. For instance, the two winters are the wettest winters for the British Isles since 1850 with rainfall totals over 500 mm (McCarthy et al., 2016).

(ii) Positive NAO and negative EA

https://doi.org/10.5194/acp-2021-797
Preprint. Discussion started: 26 October 2021

The IWV deficiencies in Southern Europe are striking in the winters of 2004/2005 and 2011/2012. This could be associated with the positive NAO and negative EA during the two winters. In this scenario, Southern Europe tends to experience colder and drier winter (Santos et al., 2013; Mellado-cano et al., 2019).

(iii) Negative NAO and positive EA

In contrast to the spatial pattern in the winter of 2011/2012, the winter of 2009/2010 witnessed pronounced IWV deficiencies in Northern Europe. The contrasting patterns of IWV anomaly could be due to the fact that the conditions of atmospheric circulations are different between these two winters, with positive NAO and negative EA in the winter of 2011/2012 but opposite phases in the winter of 2009/2010 (Santos et al., 2013). Especially the winter of 2009/2010 was marked by one of the most negative winter NAO during the last 150 years (Jung et al., 2011), which resulted in enhanced northerly surface winds towards Northern Europe from the cold and dry Arctic (Wang et al., 2010).

(iv) Both NAO and EA are negative

Northern Europe experienced a more severe IWV deficiency in the winter of 2010/2011. Comparing the December IWV anomalies of 2009 and 2010, we can find that the IWV deficiency in December 2010 is more severe. During these two December months, the NAO indices are strongly negative, indicating colder and drier-than-usual climate conditions in Northern Europe (Taws et al., 2011). However, the EA phases were slightly positive in December 2009 (Case iii here above) and negative in December 2010. Therefore, in this latter case, that negative EA strengthens the cold and dry effects due to the negative NAO, as also shown by Moore and Renfrew 2012. Therefore, the combination of negative NAO and EA indicates a more severe IWV deficiency in Northern Europe.

In addition to wintertime, the NAO and EA could also contribute to extreme IWV anomalies in other seasons. For example, Northern Europe experienced a significant negative IWV anomaly in March 2013, which could be associated with the strongly negative NAO and slightly negative EA as described in Case iv.

IWV anomalies might also be linked to other teleconnection indices (e.g., Wang et al., 2018; Thomas et al., 2021). For example, Fig. 11f illustrates that the winter IWV anomaly over Europe is well correlated with AO in a similar spatial pattern as for the NAO (Fig. 11d). This is not surprising as the AO and NAO indices are highly correlated and they are even used interchangeably in some literature (e.g., Cohen et al., 2014), albeit their definitions are different (Ambaum et al., 2001). In addition, the correlations between the winter IWV anomalies and other indices, such as the SCA, WeMO, Niño 3.4, NOI, and QBO, were also examined and displayed in Fig. 11g-k. The results show that all these indices, except for the QBO, are correlated with the winter IWV anomalies at least in some parts of Europe. However, most of their correlation coefficients are within ±0.4, hence weaker than the correlations for NAO/AO and EA. Our correlation analysis concludes that NAO/AO and EA are the dominant patterns among the teleconnection indices for the modulation of winter IWV over Europe. However, this does not mean that the other patterns might not play a role for specific extreme events. For example, the excess of IWV over Europe in the winter of 2015/2016 could also be linked to the concurrent super El Niño (ENSO) event (Stockdale et al., 2017). Moreover, although we successfully explained some of the IWV winter extremes in Europe with the four different phase combinations of NAO and EA, we must mention that the strengths and durations of the NAO and EA

https://doi.org/10.5194/acp-2021-797
Preprint. Discussion started: 26 October 2021

Atmospheric Chemistry and Physics Discussions

phase change from year to year, and that the atmospheric circulations over the Atlantic/European sector cannot be completely represented by the NAO and EA pattern. Therefore, future in-debt spatiotemporal analysis is necessary to clearly demonstrate the links between the IWV anomaly and the teleconnection indices.

The performances of the reanalyses in reproducing the interannual variations of IWV is evaluated by taking the GPS IWV anomaly as reference. The six reanalyses achieved KGE scores larger than 0.9 at most of the stations as shown in Fig. 8i. Their median KGE scores are between 0.93 and 0.97, proving that all of them are able to reproduce well the interannual IWV variations over Europe. However, the median γ scores of the six reanalyses are between 0.96 and 0.98, indicating that they slightly underestimated the variability of 1-monthly IWV anomaly. JRA55 outperforms the other reanalyses (median KGE=0.97) as it reproduces the variability of IWV anomaly the best (median γ=0.98). ERA5 only ranks second (median KGE=0.96) though it reached the highest correlation (median r=0.99). This is mostly due to its relatively lower γ (median γ=0.96). Therefore, the performance of ERA5 in reproducing the variability of monthly IWV anomaly over Europe could be further improved.

6 Assessments of trends

Figure 12a shows the trends of the monthly anomaly GPS IWV time series. The geographical pattern of the IWV trends is evident, with weaker trends in Northern Europe (generally 0-0.4 kg m^{-2} $decade^{-1}$) and larger trends in Southern Europe and the Mediterranean Sea (generally 0.4-1 kg m^{-2} $decade^{-1}$). The largest trend is found at station TUBI in Gebze, Turkey (29.5°E, 40.8°N), with a value of 1.5 kg m^{-2} $decade^{-1}$. The relative trends are characterized by a similar geographical pattern, with values from −0.5 to 8.2 % $decade^{-1}$. The geographical pattern and magnitudes of the GPS IWV trends are in line with earlier studies (Alshawaf et al., 2018; Yuan et al., 2021). The relative IWV trends derived from the reanalyses rather than their absolute trends were compared to GPS for two reasons. One reason is that the relative trend is not affected by the IWV bias. The other reason is that the relative IWV trend is related more directly to the temperature variation, with the well-known Clausius-Clapeyron relationship that states that water vapor holding capacity increases by 7% with a rise of 1 K in temperature (Trenberth et al. 2003). Figure 13 compares the relative IWV trends from the six reanalyses against GPS. The KGE score of ERA5 is 0.76, higher than all the other reanalyses' scores. It is no wonder because the ERA5 IWV time series were used for the homogenization of the GPS time series (Yuan et al., 2021). The ERAI, JRA55, and MERRA2 also achieved rather good KGE scores, with values of 0.73, 0.72, and 0.72, respectively. The results indicate that these reanalyses are also good datasets for IWV trend reproduction. However, the KGE scores of CFSR and NCEP2 are much lower, with values of 0.48 and 0.20, respectively. This is mostly due to their deficiencies in correlation (0.55 and 0.52, respectively). Moreover, NCEP2 generally overestimated the IWV trends (β=1.61).

https://doi.org/10.5194/acp-2021-797
Preprint. Discussion started: 26 October 2021

Atmospheric Chemistry and Physics Discussions

7 Conclusions

In this study, Integrated Water Vapor (IWV) time series for the period 1994-2018 were retrieved from continuous GPS observations of 108 ground-based GPS stations in Europe, with an average period of 21 years for those time series. The temporal features of Europe's IWV, such as its diurnal cycle and variation, annual cycle and interannual variation, and trend were then investigated. Moreover, the performances of six frequently used global atmospheric reanalyses in Europe were assessed for the first time, namely CFSR, ERA5, ERA-Interim (ERAI), JRA55, MERRA2, and NCEP2. The main findings are summarized here below.

(i) The agreement between the daily GPS IWV time series and the six reanalyses are found to be best for ERA5 and worst for NCEP2, with standard deviations of IWV differences of 0.5-1.6 and 1.2-3.0 kg m^{-2}, respectively. The standard deviations of IWV differences are well correlated with representativeness statistics of the six reanalyses, indicating that the representativeness differences contribute to the discrepancies between the reanalyses and GPS.

(ii) The peak-to-peak diurnal amplitudes account for 2%-18% of the associated daily mean IWV. The amplitudes are generally negatively correlated with station latitudes and positively correlated with station heights. Most of the diurnal cycles reach their minima between 5:00-12:00 Local Time (LT) and then peak around 16:00-24:00 LT. The diurnal IWV variations are much stronger than their cycles, with anomalies roughly ranging from −100% to 200% of the associated daily mean IWV. Owing to higher temporal resolutions, ERA5 and MERRA2 outperformed the other four reanalyses in reproducing 1-hourly diurnal anomalies of IWV with median KGE scores of 0.90 and 0.77, respectively. However, ERA5 slightly underperformed ERAI in modelling diurnal IWV cycles, and MERRA2 tended to overestimate the diurnal amplitudes. Further developments are needed for ERA5 and MERRA2 to enhance their capabilities in modelling the diurnal cycle of IWV.

(iii) All the monthly IWV time series are modulated with apparent annual cycles, with minima in January and February (4-17 kg m^{-2}) and maxima in July and August (17-32 kg m^{-2}). The maxima and minima of the annual cycles show consistent geographical patterns, with larger values towards the equator and at lower altitude sites. ERA5 ranks the first in modelling the annual cycles of IWV (median KGE=0.97), CFSR ranks last (median KGE=0.94) due to its overestimation of mean values (median β=1.04) and underestimation of variability (median γ=0.96).

(iv) The interannual variations of IWV over Europe are most significant in winter, with extreme values as large as ±50% of the associated monthly averages. The winter interannual variations are linked to many teleconnection patterns, especially the North Atlantic Oscillation (NAO) and East Atlantic (EA) pattern. The NAO positive (negative) phase in winter indicates an enhanced (deficient) IWV in Northern Europe and a deficient (enhanced) IWV in Southern Europe. The winter phase of the EA pattern is positively correlated with the IWV anomaly over Europe. All the six renalyses are capable of reproducing the interannual variations very well, with most of their KGE scores larger than 0.9. However, they slightly underestimate the magnitudes of the extreme values with median γ ranging from 0.96 to 0.99.

https://doi.org/10.5194/acp-2021-797
Preprint. Discussion started: 26 October 2021

Atmospheric Chemistry and Physics Discussions

(v) Europe's IWV is increasing as observed from more than two decades of continuous GPS observations. The trends are generally 0-0.4 kg m^{-2} $decade^{-1}$ in Northern Europe, such as Iceland, British Isles, Fennoscandian Peninsula, Jutland Peninsula, and the western and northern coastal regions of the central European mainland. Stronger IWV trends (generally 0.4-1 kg m^{-2} $decade^{-1}$) are observed in Southern Europe, i.e., the Iberian Peninsula, the Italian Peninsula, the Balkan Peninsula, and the islands in the Mediterranean Sea. The largest trend is found at station TUBI in Gebze, Turkey (29.5°E, 40.8°N), with a value of 1.5 kg m^{-2} $decade^{-1}$. ERA5 achieves the best consistency with GPS IWV trends (KGE=0.76) but it has been used to homogenize the GPS IWV time series. In contrast, NCEP performs the worst in reproducing the IWV trends (KGE=0.20) primarily because of its pronounced overestimation of the IWV trends (β=1.61) and relatively poor correlation with the GPS trends (r=0.52).

Overall, it can be concluded that the reanalyses successfully reproduce the spatiotemporal IWV variability over Europe, as assessed with the GPS IWV dataset, with ERA5 slightly outperforming the other reanalyses at most temporal scales. Due to lack of accurate and complete *in-situ* meteorological observations at the GPS stations, pressure and weighted mean temperature obtained from ERA5 were used in the conversion of GPS ZTD to IWV. This could partly contribute to the superior agreement between the IWV from ERA5 and GPS. Future studies could validate the IWV products of reanalyses using ground-based GPS when independent, quality-assured, and complete meteorological observations at the GPS stations are available. IWV measurements from other techniques could also be helpful.

Data availability. The GPS ZTD data were provided by NGL (http://geodesy.unr.edu). The ERA5 and ERAI data were downloaded from the climate data store (https://cds.climate.copernicus.eu) and ECWMF (https://www.ecmwf.int), respectively. The CFSR and JRA55 data are available in the research data archive of NCAR (https://rda.ucar.edu). MERRA2 data were derived from NASA Goddard earth sciences data and information services center (https://disc.gsfc.nasa.gov). NCEP2 data were obtained from NOAA/OAR/ESRL physical sciences laboratory (https://psl.noaa.gov). The AO, EA, NAO, Niño 3.4, and SCA indices were provided by the Climate Prediction Center (CPC) of NOAA (https://www.cpc.ncep.noaa.gov). The NOI, QBO, and WeMO indices were obtained from the Environmental Research Division (ERD) of NOAA (https://oceanview.pfeg.noaa.gov), the Physical Sciences Laboratory (PSL) of NOAA (https://www.cpc.ncep.noaa.gov), and the Climatology Group of University of Barcelona (http://www.ub.edu/gc/wemo), respectively. The GNSS IWV time series are available from the corresponding author upon reasonable request.

Author contributions. PY: Conceptualization, Methodology, Formal analysis, Investigation, Writing Original Draft, and Visualization. RV, XY, HV, JA, and BH: Investigation and Reviewing. HK: Investigation, Reviewing, Supervision, Project administration, and Funding acquisition.

Competing interests. The authors declare that they have no competing interests.

Acknowledgements. We are grateful to NGL for providing the GPS ZTD products and many institutions for sharing the continuous GPS observations. We thank ECMWF, JMA, NASA GAMO, and NCEP for providing the reanalyses products.

https://doi.org/10.5194/acp-2021-797
Preprint. Discussion started: 26 October 2021

Atmospheric Chemistry and Physics Discussions

475 We also would like to thank the CPC, ERD, and PSL of NOAA, as well as the Climatology Group of University of Barcelona for providing the climate indices. This work was performed under the German Research Foundation (DFG, project number: 321886779).

https://doi.org/10.5194/acp-2021-797
Preprint. Discussion started: 26 October 2021

Atmospheric Chemistry and Physics Discussions

References

Alshawaf, F., Zus, F., Balidakis, K., Deng, Z., Hoseini, M., Dick, G., and Wickert, J.: On the statistical significance of climatic trends estimated from GPS tropospheric time series, Journal of Geophysical Research: Atmospheres, 123, 10–967, 2018.

Ambaum, M. H., Hoskins, B. J., and Stephenson, D. B.: Arctic oscillation or North Atlantic oscillation?, Journal of Climate, 14, 3495–3507, 2001.

Ao, C. O., Meehan, T., Hajj, G., Mannucci, A., and Beyerle, G.: Lower troposphere refractivity bias in GPS occultation retrievals, Journal of Geophysical Research: Atmospheres, 108, 2003.

Awange, J. L.: Environmental monitoring using GNSS: Global navigation satellite systems, . Springer-Verlag, Berlin, Heidelberge, New York., 2012.

Awange, J. L.: GNSS environmental sensing, Springer International Publishers, 2018.

Baldwin, M., Gray, L., Dunkerton, T., Hamilton, K., Haynes, P., Randel, W., Holton, J., Alexander, M., Hirota, I., and Horinouchi, T.: The quasi-biennial oscillation, Reviews of Geophysics, 39, 179–229, 2001.

Barnston, A. G. and Livezey, R. E.: Classification, seasonality and persistence of low-frequency atmospheric circulation patterns, Monthly weather review, 115, 1083–1126, 1987.

Bernet, L., Brockmann, E., von Clarmann, T., Kämpfer, N., Mahieu, E., Mätzler, C., Stober, G., and Hocke, K.: Trends of atmospheric water vapour in Switzerland from ground-based radiometry, FTIR and GNSS data, Atmospheric Chemistry and Physics, 20, 11 223–11 244, 2020.

Bertiger, W., Bar-Sever, Y., Dorsey, A., Haines, B., Harvey, N., Hemberger, D., Heflin, M., Lu, W., Miller, M., and Moore, A. W.: GipsyX/RTGx, a new tool set for space geodetic operations and research, Advances in Space Research, 66, 469–489, 2020.

Bevis, M., Businger, S., Chiswell, S., Herring, T. A., Anthes, R. A., Rocken, C., and Ware, R. H.: GPS meteorology: Mapping zenith wet delays onto precipitable water, Journal of applied meteorology, 33, 379–386, 1994.

Bevis, M., Businger, S., Herring, T. A., Rocken, C., Anthes, R. A., and Ware, R. H.: GPS meteorology: Remote sensing of atmospheric water vapor using the Global Positioning System, Journal of Geophysical Research: Atmospheres, 97, 15787–15801, 1992.

Blewitt, G., Hammond, W. C., and Kreemer, C.: Harnessing the GPS data explosion for interdisciplinary science, Eos, 99, 485, 2018.

Bock, O. and Parracho, A. C.: Consistency and representativeness of integrated water vapour from ground-based GPS observations and ERA-Interim reanalysis, Atmospheric Chemistry and Physics, 19, 9453–9468, 2019.

Bock, O., Keil, C., Richard, E., Flamant, C., and Bouin, M.: Validation of precipitable water from ECMWF model analyses with GPS and radiosonde data during the MAP SOP, Quarterly Journal of the Royal Meteorological Society: A journal of the atmospheric sciences, applied meteorology and physical oceanography, 131, 3013–3036, 2005.

https://doi.org/10.5194/acp-2021-797
Preprint. Discussion started: 26 October 2021

Boehm, J., Werl, B., and Schuh, H.: Troposphere mapping functions for GPS and very long baseline interferometry from European Centre for Medium-Range Weather Forecasts operational analysis data, Journal of geophysical research: solid earth, 111, 2006.

Bonafoni, S., Biondi, R., Brenot, H., and Anthes, R.: Radio occultation and ground-based GNSS products for observing, understanding and predicting extreme events: A review, Atmospheric research, 230, 104624, 2019.

Bruyninx, C., Habrich, H., Söhne, W., Kenyeres, A., Stangl, G., and Völksen, C.: Enhancement of the EUREF permanent network services and products, in: Geodesy for planet Earth, Springer, 27–34, 2012.

Chen, B. and Liu, Z.: Global water vapor variability and trend from the latest 36 year (1979 to 2014) data of ECMWF and NCEP reanalyses, radiosonde, GPS, and microwave satellite, Journal of Geophysical Research: Atmospheres, 121, 11 442-11 462, 2016.

Cohen, J., Screen, J. A., Furtado, J. C., Barlow, M., Whittleston, D., Coumou, D., Francis, J., Dethloff, K., Entekhabi, D., and Overland, J.: Recent Arctic amplification and extreme mid-latitude weather, Nature geoscience, 7, 627–637, 2014.

Comas-Bru, L. and McDermott, F.: Impacts of the EA and SCA patterns on the European twentieth century NAO–winter climate relationship, Quarterly Journal of the Royal Meteorological Society, 140, 354–363, 2014.

Copernicus: European State of the Climate 2019 | Copernicus: https://climate.copernicus.eu/ESOTC/2019, last access: 20 September 2021.

Dai, A., Wang, J., Thorne, P. W., Parker, D. E., Haimberger, L., and Wang, X. L.: A new approach to homogenize daily radiosonde humidity data, Journal of Climate, 24, 965–991, 2011.

Dai, A., Wang, J., Ware, R. H., and Van Hove, T.: Diurnal variation in water vapor over North America and its implications for sampling errors in radiosonde humidity, Journal of Geophysical Research: Atmospheres, 107, ACL-11, 2002.

Davis, J., Herring, T., Shapiro, I., Rogers, A., and Elgered, G.: Geodesy by radio interferometry: Effects of atmospheric modeling errors on estimates of baseline length, Radio science, 20, 1593–1607, 1985.

Dee, D. P., Uppala, S. M., Simmons, A., Berrisford, P., Poli, P., Kobayashi, S., Andrae, U., Balmaseda, M., Balsamo, G., and Bauer, d P.: The ERA-Interim reanalysis: Configuration and performance of the data assimilation system, Quarterly Journal of the royal meteorological society, 137, 553–597, 2011.

Diedrich, H., Wittchen, F., Preusker, R., and Fischer, J.: Representativeness of total column water vapour retrievals from instruments on polar orbiting satellites, Atmospheric Chemistry and Physics, 16, 8331–8339, 2016.

Drobinski, P., Bastin, S., Arsouze, T., Beranger, K., Flaounas, E., and Stefanon, M.: North-western Mediterranean sea-breeze circulation in a regional climate system model, Climate Dynamics, 51, 1077–1093, 2018.

Durre, I., Williams Jr, C. N., Yin, X., and Vose, R. S.: Radiosonde-based trends in precipitable water over the Northern Hemisphere: An update, Journal of Geophysical Research: Atmospheres, 114, 2009.

Durre, I., Yin, X., Vose, R. S., Applequist, S., and Arnfield, J.: Enhancing the data coverage in the Integrated Global Radiosonde Archive, Journal of Atmospheric and Oceanic Technology, 35, 1753–1770, 2018.

https://doi.org/10.5194/acp-2021-797
Preprint. Discussion started: 26 October 2021

Ejigu, Y. G., Teferle, F. N., Klos, A., Janusz, B., and Hunegnaw, A.: Monitoring and prediction of hurricane tracks using GPS tropospheric products, GPS Solutions, 25, 1–15, 2021.

Fadnavis, S., Müller, R., Chakraborty, T., Sabin, T. P., Laakso, A., Rap, A., Griessbach, S., Vernier, J.-P., and Tilmes, S.: The role of tropical volcanic eruptions in exacerbating Indian droughts, Scientific Reports, 11, 2714, 2021.

Field, C. B. and Barros, V. R.: Climate change 2014–Impacts, adaptation and vulnerability: Regional aspects, Cambridge University Press, 2014.

Gelaro, R., McCarty, W., Suárez, M. J., Todling, R., Molod, A., Takacs, L., Randles, C. A., Darmenov, A., Bosilovich, M. G., and Reichle, R.: The modern-era retrospective analysis for research and applications, version 2 (MERRA-2), Journal of climate, 30, 5419–5454, 2017.

Grossi, M., Valks, P., Loyola, D., Aberle, B., Slijkhuis, S., Wagner, T., Beirle, S., and Lang, R.: Total column water vapour measurements from GOME-2 MetOp-A and MetOp-B, 8, 1111–1133, Atmospheric Measurement Techniques, 2015.

Gupta, H. V., Kling, H., Yilmaz, K. K., and Martinez, G. F.: Decomposition of the mean squared error and NSE performance criteria: Implications for improving hydrological modelling, Journal of hydrology, 377, 80–91, 2009.

Hagemann, S., Bengtsson, L., and Gendt, G.: On the determination of atmospheric water vapor from GPS measurements, Journal of Geophysical Research: Atmospheres, 108, 2003.

Held, I. M. and Soden, B. J.: Water vapor feedback and global warming, Annual review of energy and the environment, 25, 441–475, 2000.

Hersbach, H., Bell, B., Berrisford, P., Hirahara, S., Horányi, A., Muñoz-Sabater, J., Nicolas, J., Peubey, C., Radu, R., and Schepers, D.: The ERA5 global reanalysis, Quarterly Journal of the Royal Meteorological Society, 146, 1999–2049, 2020.

Huang, L., Peng, H., Liu, L., Xiong, S., Xie, S., Chen, J., Li, J., and He, H.: GNSS Precipitable Water Vapor Retrieval with the Aid of NWM Data for China, Earth and Space Science, 8, e2020EA001550, 2021.

Hurrell, J. W.: Decadal trends in the North Atlantic Oscillation: Regional temperatures and precipitation, Science, 269, 676–679, 1995.

Jade, S. and Vijayan, M.: GPS-based atmospheric precipitable water vapor estimation using meteorological parameters interpolated from NCEP global reanalysis data, Journal of Geophysical Research: Atmospheres, 113, 2008.

Jiang, W., Yuan, P., Chen, H., Cai, J., Li, Z., Chao, N., and Sneeuw, N.: Annual variations of monsoon and drought detected by GPS: A case study in Yunnan, China, Scientific reports, 7, 1–10, 2017.

Jones, J., Guerova, G., Douša, J., Dick, G., de Haan, S., Pottiaux, E., Bock, O., Pacione, R., and van Malderen, R. (Eds.): Advanced GNSS Tropospheric Products for Monitoring Severe Weather Events and Climate: COST Action ES1206 Final Action Dissemination Report, Springer International Publishing, Cham, 2020.Jones, J., Guerova, G., Douša, J., Dick, G., de Haan, S., Pottiaux, E., and Van Malderen, R.: Advanced GNSS tropospheric products for monitoring severe weather events and climate, COST action ES1206 final action dissemination report, 563, 2019.

https://doi.org/10.5194/acp-2021-797
Preprint. Discussion started: 26 October 2021

Jung, T., Vitart, F., Ferranti, L., and Morcrette, J.: Origin and predictability of the extreme negative NAO winter of 2009/10, Geophysical Research Letters, 38, 2011.

Kämpfer, N. (Ed.): Monitoring Atmospheric Water Vapour: Ground-Based Remote Sensing and In-situ Methods, ISSI Scientific Reports Series, Vol. 10, ISBN 978-1-4614-3908-0, Springer, Berlin, Heidelberg, New York, 2012.

Kanamitsu, M., Ebisuzaki, W., Woollen, J., Yang, S.-K., Hnilo, J., Fiorino, M., and Potter, G.: Ncep–doe amip-ii reanalysis (r-2), Bulletin of the American Meteorological Society, 83, 1631–1644, 2002.

Khutorova, O., Khutorov, V., and Teptin, G.: Interannual variability of surface and integrated water vapor and atmospheric circulation in Europe, Atmospheric and Oceanic Optics, 31, 486–491, 2018.

Kiehl, J. T. and Trenberth, K. E.: Earth's annual global mean energy budget, Bulletin of the American meteorological society, 78, 197–208, 1997.

Kling, H., Fuchs, M., and Paulin, M.: Runoff conditions in the upper Danube basin under an ensemble of climate change scenarios, Journal of Hydrology, 424, 264–277, 2012.

Kobayashi, S., Ota, Y., Harada, Y., Ebita, A., Moriya, M., Onoda, H., Onogi, K., Kamahori, H., Kobayashi, C., and Endo, H.: The JRA-55 reanalysis: General specifications and basic characteristics, Journal of the Meteorological Society of Japan. Ser. II, 93, 5–48, 2015.

Krämer, M., Rolf, C., Spelten, N., Afchine, A., Fahey, D., Jensen, E., Khaykin, S., Kuhn, T., Lawson, P., Lykov, A., Pan, L. L., Riese, M., Rollins, A., Stroh, F., Thornberry, T., Wolf, V., Woods, S., Spichtinger, P., Quaas, J., and Sourdeval, O.: A microphysics guide to cirrus – Part 2: Climatologies of clouds and humidity from observations, Atmospheric Chemistry and Physics, 20, 12 569–12 608, 2020.

Kunz, A., Müller, R., Homonnai, V., M. Jánosi, I., Hurst, D., Rap, A., M. Forster, P., Rohrer, F., Spelten, N., and Riese, M.: Extending water vapor trend observations over Boulder into the tropopause region: Trend uncertainties and resulting radiative forcing, Journal of Geophysical Research: Atmospheres, 118, 11 269–11 284, 2013.

Kunz, A., Spelten, N., Konopka, P., Müller, R., Forbes, R. M., and Wernli, H.: Comparison of Fast In situ Stratospheric Hygrometer (FISH) measurements of water vapor in the upper troposphere and lower stratosphere (UTLS) with ECMWF (re)analysis data, Atmospheric Chemistry and Physics, 14, 10 803–10 822, 2014.

Kursinski, E., Hajj, G., Hardy, K., Romans, L., and Schofield, J.: Observing tropospheric water vapor by radio occultation using the Global Positioning System, Geophysical Research Letters, 22, 2365–2368, 1995.

Lavers, D. A., Pappenberger, F., Richardson, D. S., and Zsoter, E.: ECMWF Extreme Forecast Index for water vapor transport: A forecast tool for atmospheric rivers and extreme precipitation, Geophysical Research Letters, 43, 11–852, 2016.

Martin-Vide, J. and Lopez-Bustins, J.: The western Mediterranean oscillation and rainfall in the Iberian Peninsula, International Journal of Climatology: A Journal of the Royal Meteorological Society, 26, 1455–1475, 2006.

McCarthy, M. P., Thorne, P., and Titchner, H. A.: An analysis of tropospheric humidity trends from radiosondes, Journal of Climate, 22, 5820–5838, 2009.

https://doi.org/10.5194/acp-2021-797
Preprint. Discussion started: 26 October 2021

Atmospheric Chemistry and Physics Discussions

McCarthy, M., Spillane, S., Walsh, S., and Kendon, M.: The meteorology of the exceptional winter of 2015/2016 across the UK and Ireland, Weather, 71, 305–313, 2016.

Mellado-Cano, J., Barriopedro, D., García-Herrera, R., Trigo, R. M., and Hernández, A.: Examining the North Atlantic oscillation, East Atlantic Pattern, and jet variability since 1685, Journal of Climate, 32, 6285–6298, 2019.

Mikhailova, N. and Yurovsky, A.: The East Atlantic oscillation: mechanism and impact on the European climate in winter, Physical Oceanography, 2016.

Moore, G. and Renfrew, I.: Cold European winters: interplay between the NAO and the East Atlantic mode, Atmospheric Science Letters, 13, 1–8, 2012.

Mueller, B. and Seneviratne, S. I.: Systematic land climate and evapotranspiration biases in CMIP5 simulations, Geophysical research letters, 41, 128–134, 2014.

Müller, R., Kunz, A., Hurst, D. F., Rolf, C., Krämer, M., and Riese, M.: The need for accurate long-term measurements of water vapor in the upper troposphere and lower stratosphere with global coverage, Earth's Future, 4, 25–32, 2016.

Nilsson, T. and Elgered, G.: Long-term trends in the atmospheric water vapor content estimated from ground-based GPS data, Journal of Geophysical Research: Atmospheres, 113, 2008.

Ning, T., Wickert, J., Deng, Z., Heise, S., Dick, G., Vey, S., and Schöne, T.: Homogenized time series of the atmospheric water vapor content obtained from the GNSS reprocessed data, Journal of Climate, 29, 2443–2456, 2016.

Parracho, A. C., Bock, O., and Bastin, S.: Global IWV trends and variability in atmospheric reanalyses and GPS observations, Atmospheric Chemistry and Physics, 18, 16213–16237, 2018.

Randel, W. J. and Wu, F.: Kelvin wave variability near the equatorial tropopause observed in GPS radio occultation measurements, Journal of Geophysical Research: Atmospheres, 110, 2005.

Randel, W. J., Wu, F., and Forster, P.: The Extratropical Tropopause Inversion Layer: Global Observations with GPS Data, and a Radiative Forcing Mechanism, Journal of the Atmospheric Sciences., 64, 4489–4496, 2007.

Rebischung, P. and Schmid, R.: IGS14/igs14. atx: a new framework for the IGS products, AGU Fall Meeting 2016, 2016.

Saastamoinen, J.: Atmospheric correction for the troposphere and stratosphere in radio ranging satellites, The use of artificial satellites for geodesy, 15, 247–251, 1972.

Saha, S., Moorthi, S., Pan, H.-L., Wu, X., Wang, J., Nadiga, S., Tripp, P., Kistler, R., Woollen, J., and Behringer, D.: The NCEP climate forecast system reanalysis, Bulletin of the American Meteorological Society, 91, 1015–1058, 2010.

Saha, S., Moorthi, S., Wu, X., Wang, J., Nadiga, S., Tripp, P., Behringer, D., Hou, Y.-T., Chuang, H., and Iredell, M.: The NCEP climate forecast system version 2, Journal of climate, 27, 2185–2208, 2014.

Santos, J. A., Woollings, T., and Pinto, J. G.: Are the winters 2010 and 2012 archetypes exhibiting extreme opposite behavior of the North Atlantic jet stream?, Monthly Weather Review, 141, 3626–3640, 2013.

Schneider, T., O'Gorman, P. A., and Levine, X. J.: Water vapor and the dynamics of climate changes, Reviews of Geophysics, 48, 2010.

https://doi.org/10.5194/acp-2021-797
Preprint. Discussion started: 26 October 2021

645 Schröder, M., Lockhoff, M., Fell, F., Forsythe, J., Trent, T., Bennartz, R., Borbas, E., Bosilovich, M. G., Castelli, E., and Hersbach, H.: The GEWEX Water Vapor Assessment archive of water vapour products from satellite observations and reanalyses, Earth system science data, 10, 1093–1117, 2018.

Schröder, M., Lockhoff, M., Forsythe, J. M., Cronk, H. Q., Vonder Haar, T. H., and Bennartz, R.: The GEWEX water vapor assessment: Results from intercomparison, trend, and homogeneity analysis of total column water vapor, Journal of
650 Applied Meteorology and Climatology, 55, 1633–1649, 2016.

Schüler, T.: On ground-based GPS tropospheric delay estimation (PhD Thesis), Univ. der Bundeswehr München, Fak. für Bauingenieur-und Vermessungswesen, Studiengang Geodäsie und Geoinformation, 2001.

Schwing, F., Murphree, T., and Green, P.: The Northern Oscillation Index (NOI): a new climate index for the northeast Pacific, Progress in Oceanography, 53, 115–139, 2002.

655 Sharifnezhadazizi, Z., Norouzi, H., Prakash, S., Beale, C., and Khanbilvardi, R.: A global analysis of land surface temperature diurnal cycle using MODIS observations, Journal of Applied Meteorology and Climatology, 58, 1279–1291, 2019.

Steinke, S., Wahl, S., and Crewell, S.: Benefit of high resolution COSMO reanalysis: The diurnal cycle of column-integrated water vapor over Germany, Meteorol. Z, 28, 165–177, 2019.

660 Stockdale, T., Balmaseda, M., and Ferranti, L.: The 2015/2016 El Niño and beyond. ECMWF Newsletter 151, 464–465, 2017.

Taws, S. L., Marsh, R., Wells, N. C., and Hirschi, J.: Re-emerging ocean temperature anomalies in late-2010 associated with a repeat negative NAO, Geophysical Research Letters, 38, 2011.

Thébault, E., Finlay, C. C., Beggan, C. D., Alken, P., Aubert, J., Barrois, O., Bertrand, F., Bondar, T., Boness, A., and
665 Brocco, L.: International geomagnetic reference field: the 12th generation, Earth, Planets and Space, 67, 1–19, 2015.

Thompson, D. W. and Wallace, J. M.: The Arctic Oscillation signature in the wintertime geopotential height and temperature fields, Geophysical research letters, 25, 1297–1300, 1998.

Tilmes, S., Pan, L. L., Hoor, P., Atlas, E., Avery, M. A., Campos, T., Christensen, L. E., Diskin, G. S., Gao, R.-S., Herman, R. L., Hintsa, E. J., Loewenstein, M., Lopez, J., Paige, M. E., Pittman, J. V., Podolske, J. R., Proffitt, M. R., Sachse, G.
670 W., Schiller, C., Schlager, H., Smith, J., Spelten, N., Webster, C., Weinheimer, A., and Zondlo, M. A.: An aircraft-based upper troposphere lower stratosphere O3, CO, and H2O climatology for the Northern Hemisphere, Journal of Geophysical Research: Atmospheres, 115, D14303, 2010.

Trenberth, K. E. and Fasullo, J. T.: North American water and energy cycles, Geophysical research letters, 40, 365–369, 2013.

675 Trenberth, K. E., Dai, A., Rasmussen, R. M., and Parsons, D. B.: The changing character of precipitation, Bulletin of the American Meteorological Society, 84, 1205–1218, 2003.

Trenberth, K. E.: Framing the way to relate climate extremes to climate change, Climatic change, 115, 283–290, 2012.

Trenberth, K. E.: The definition of el nino, Bulletin of the American Meteorological Society, 78, 2771–2778, 1997.

https://doi.org/10.5194/acp-2021-797
Preprint. Discussion started: 26 October 2021

Trigo, R. M., Osborn, T. J., and Corte-Real, J. M.: The North Atlantic Oscillation influence on Europe: climate impacts and associated physical mechanisms, Climate research, 20, 9–17, 2002.

Turato, B., Reale, O., and Siccardi, F.: Water vapor sources of the October 2000 Piedmont flood, Journal of Hydrometeorology, 5, 693–712, 2004.

Van Malderen, R., Pottiaux, E., Klos, A., Domonkos, P., Elias, M., Ning, T., Bock, O., Guijarro, J., Alshawaf, F., and Hoseini, M.: Homogenizing GPS integrated water vapor time series: Benchmarking break detection methods on synthetic data sets, Earth and Space Science, 7, e2020EA001121, 2020.

Vey, S., Dietrich, R., Rülke, A., Fritsche, M., Steigenberger, P., and Rothacher, M.: Validation of precipitable water vapor within the NCEP/DOE reanalysis using global GPS observations from one decade, Journal of Climate, 23, 1675–1695, 2010.

Vogelmann, H., Sussmann, R., Trickl, T., and Reichert, A.: Spatiotemporal variability of water vapor investigated using lidar and FTIR vertical soundings above the Zugspitze, Atmospheric Chemistry and Physics, 15, 3135–3148, 2015.

Vonder Haar, T. H., Bytheway, J. L., and Forsythe, J. M.: Weather and climate analyses using improved global water vapor observations, Geophysical Research Letters, 39, 2012.

Wagner, T., Beirle, S., Dörner, S., Borger, C., and Van Malderen, R.: Identification of atmospheric and oceanic teleconnection patterns in a 20-year global data set of the atmospheric water vapour column measured from satellites in the visible spectral range, Atmospheric Chemistry and Physics, 21, 5315–5353, 2021.

Wang, C., Liu, H., and Lee, S.: The record-breaking cold temperatures during the winter of 2009/2010 in the Northern Hemisphere, Atmospheric Science Letters, 11, 161–168, 2010.

Wang, J. and Zhang, L.: Climate applications of a global, 2-hourly atmospheric precipitable water dataset derived from IGS tropospheric products, Journal of Geodesy, 83, 209–217, 2009.

Wang, J., Dai, A., and Mears, C.: Global water vapor trend from 1988 to 2011 and its diurnal asymmetry based on GPS, radiosonde, and microwave satellite measurements, Journal of Climate, 29, 5205–5222, 2016.

Wang, J., Zhang, L., and Dai, A.: Global estimates of water-vapor-weighted mean temperature of the atmosphere for GPS applications, Journal of Geophysical Research: Atmospheres, 110, 2005.

Wang, S., Xu, T., Nie, W., Jiang, C., Yang, Y., Fang, Z., Li, M., and Zhang, Z.: Evaluation of precipitable water vapor from five reanalysis products with Ground-Based GNSS observations, Remote Sensing, 12, 1817, 2020.

Wang, X., Zhang, K., Wu, S., Li, Z., Cheng, Y., Li, L., and Yuan, H.: The correlation between GNSS-derived precipitable water vapor and sea surface temperature and its responses to El Niño–Southern Oscillation, Remote Sensing of Environment, 216, 1–12, 2018.

Wang, Y., Yang, K., Pan, Z., Qin, J., Chen, D., Lin, C., Chen, Y., Tang, W., Han, M., and Lu, N.: Evaluation of precipitable water vapor from four satellite products and four reanalysis datasets against GPS measurements on the Southern Tibetan Plateau, Journal of Climate, 30, 5699–5713, 2017.

https://doi.org/10.5194/acp-2021-797
Preprint. Discussion started: 26 October 2021

Wypych, A., Bochenek, B., and Różycki, M.: Atmospheric moisture content over Europe and the Northern Atlantic, Atmosphere, 9, 18, 2018.

Yuan, P., Hunegnaw, A., Alshawaf, F., Awange, J., Klos, A., Teferle, F. N., and Kutterer, H.: Feasibility of ERA5 integrated water vapor trends for climate change analysis in continental Europe: An evaluation with GPS (1994–2019) by considering statistical significance, Remote Sensing of Environment, 260, 112416, 2021.

https://doi.org/10.5194/acp-2021-797
Preprint. Discussion started: 26 October 2021

Atmospheric Chemistry and Physics Discussions

Zhu, Y. and Newell, R. E.: Atmospheric rivers and bombs, Geophysical Research Letters, 21, 1999–2002, 1994.

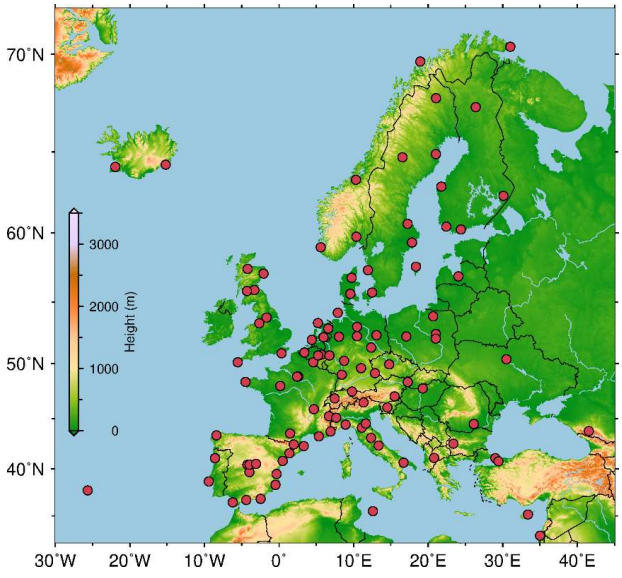

Figure 1. Geographical distribution of the 108 GPS stations (red dots). An enlarged version of this figure with station names is provided in Figure S1 in the supplementary material. The coordinates of the stations and their time lengths are provided in Table S1.

https://doi.org/10.5194/acp-2021-797
Preprint. Discussion started: 26 October 2021

Atmospheric Chemistry and Physics Discussions

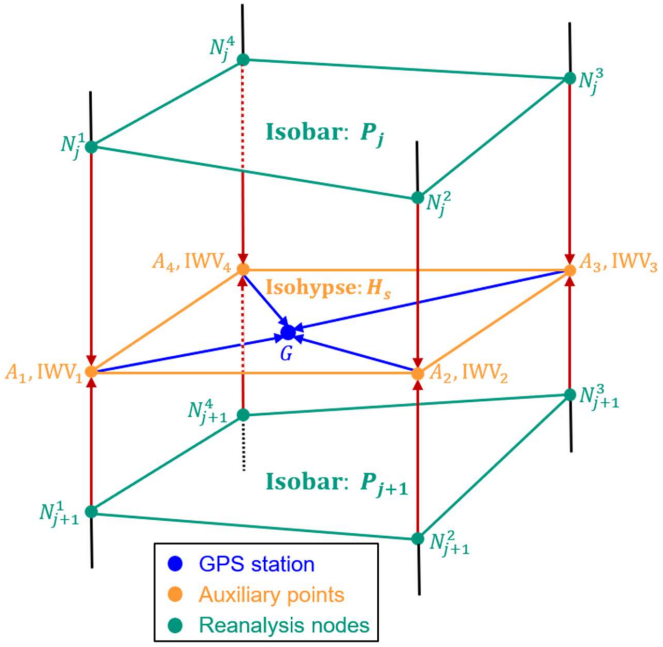

725 **Figure 2.** Schematic plot of the vertical and horizontal interpolation of the reanalysis pressure level products. The IWV at each auxiliary point (A_i; orange dots) is calculated with vertical inter- /extrapolation of the reanalysis nodes (N_j^i; green dots). The IWV at the GPS station G is then estimated with horizontal interpolation of the auxiliary points.

https://doi.org/10.5194/acp-2021-797
Preprint. Discussion started: 26 October 2021

Atmospheric Chemistry and Physics Discussions

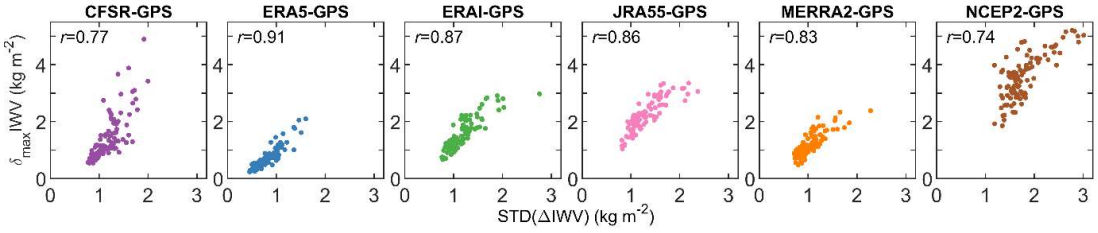

730 **Figure 3.** Scatterplots showing the relationships between the standard deviations of daily IWV difference (reanalyses minus GPS) and the representativeness error statistics for the 108 GPS stations.

https://doi.org/10.5194/acp-2021-797
Preprint. Discussion started: 26 October 2021

Atmospheric Chemistry and Physics Discussions

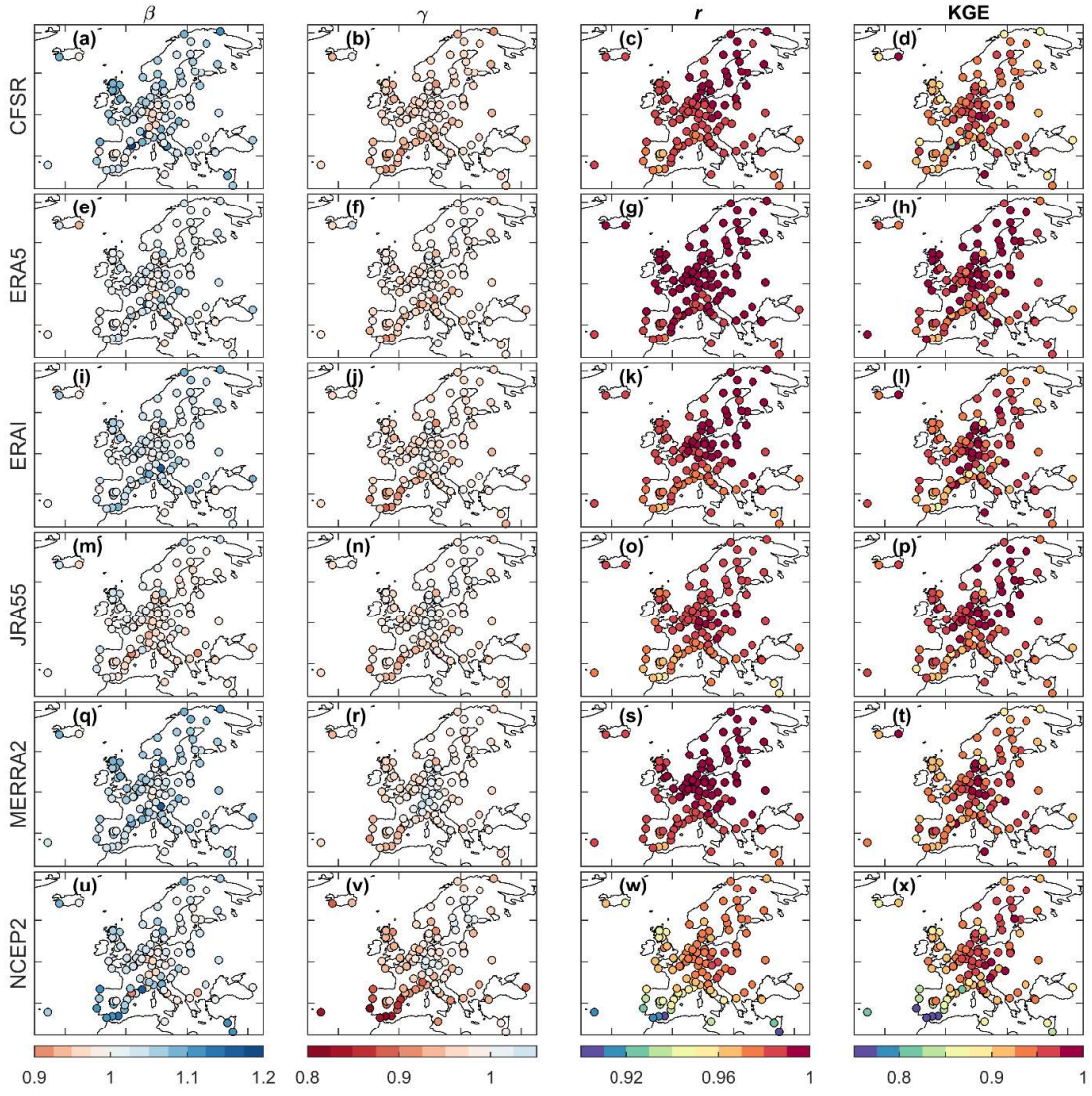

Figure 4. Plots of the KGE parameters for the daily IWV time series of the 108 GPS stations. The β and γ indicate the consistencies in the mean and variability, respectively. The r indicates the Pearson correlation coefficient between the GPS and reanalyses time series. With perfect consistencies in mean, variability, and correlation, the β, γ, and r are identical to 1, respectively. When the β, γ, and r are identical to 1, the KGE score will reach its maximum value of 1.

https://doi.org/10.5194/acp-2021-797
Preprint. Discussion started: 26 October 2021

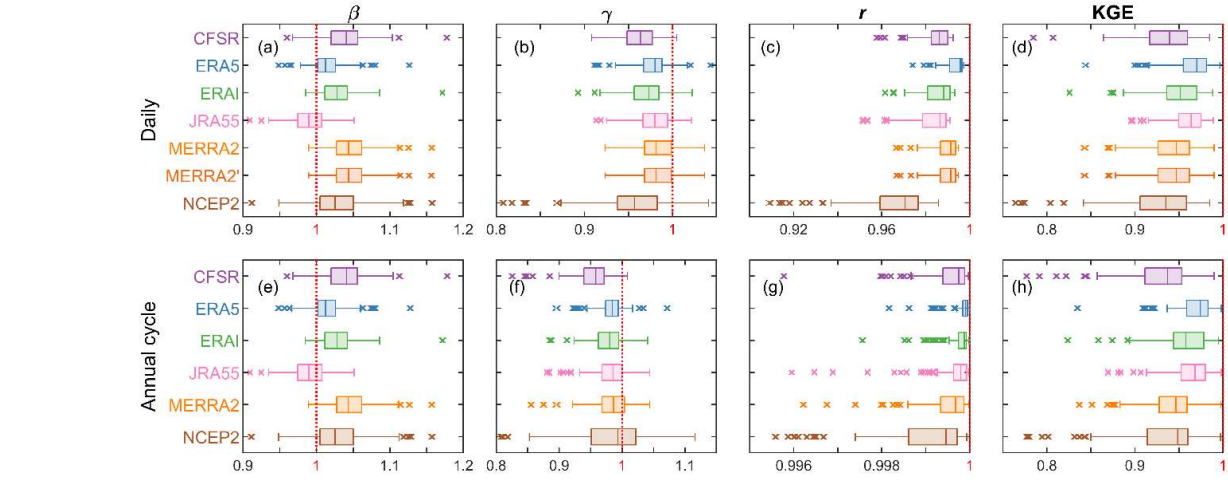

Figure 5. Box-whisker plots of the KGE parameters for the daily time series (a-d) and monthly annual cycle of IWV (e-h) from the reanalyses compared to GPS for the 108 stations.

https://doi.org/10.5194/acp-2021-797
Preprint. Discussion started: 26 October 2021

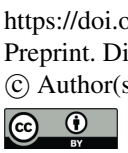

Atmospheric Chemistry and Physics Discussions

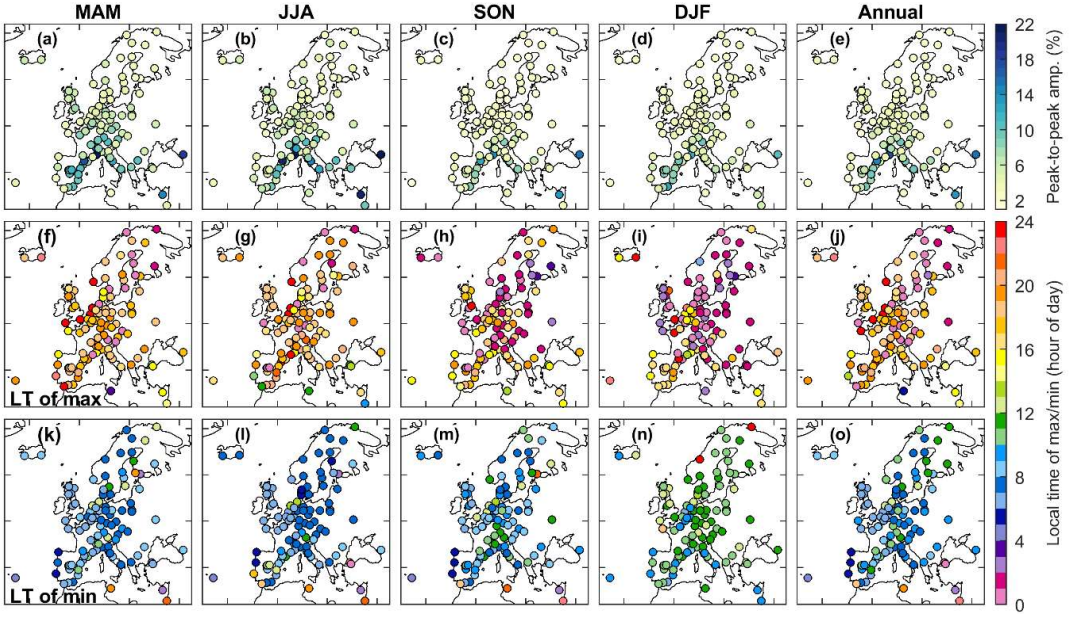

Figure 6. Plots of the relative peak-to-peak amplitude (a), local time of occurrence of the maximum (f) and minimum (k) of the diurnal cycle of GPS IWV averaged in MAM (spring) for the 108 GPS stations. The other subplots are for JJA (summer), SON (autumn), DJF (winter), and annual, from left to right, respectively.

https://doi.org/10.5194/acp-2021-797
Preprint. Discussion started: 26 October 2021

Atmospheric Chemistry and Physics Discussions

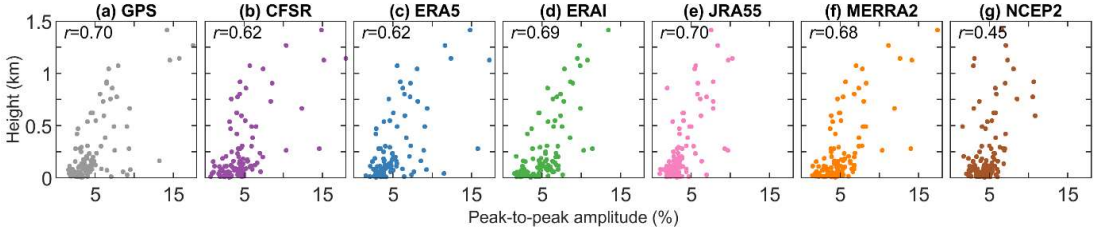

Figure 7. Comparison of the peak-to-peak amplitude of the relative diurnal cycle of IWV and station height for the 108 GPS stations. (a-g) are for the IWV from GPS and various reanalyses, respectively.

750

https://doi.org/10.5194/acp-2021-797
Preprint. Discussion started: 26 October 2021

Atmospheric Chemistry and Physics Discussions

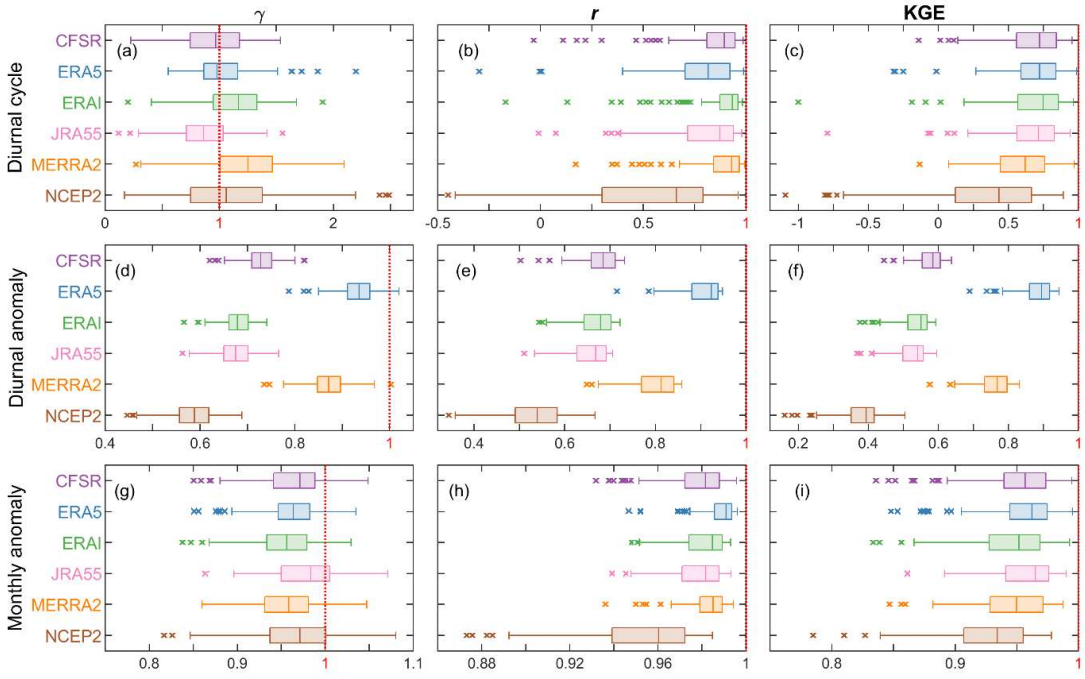

Figure 8. Box-whisker plots of the KGE parameters for the relative diurnal cycle (a-c), diurnal anomaly (d-f), and monthly anomaly (g-i) of IWV from the reanalyses compared to GPS for the 108 stations.

https://doi.org/10.5194/acp-2021-797
Preprint. Discussion started: 26 October 2021

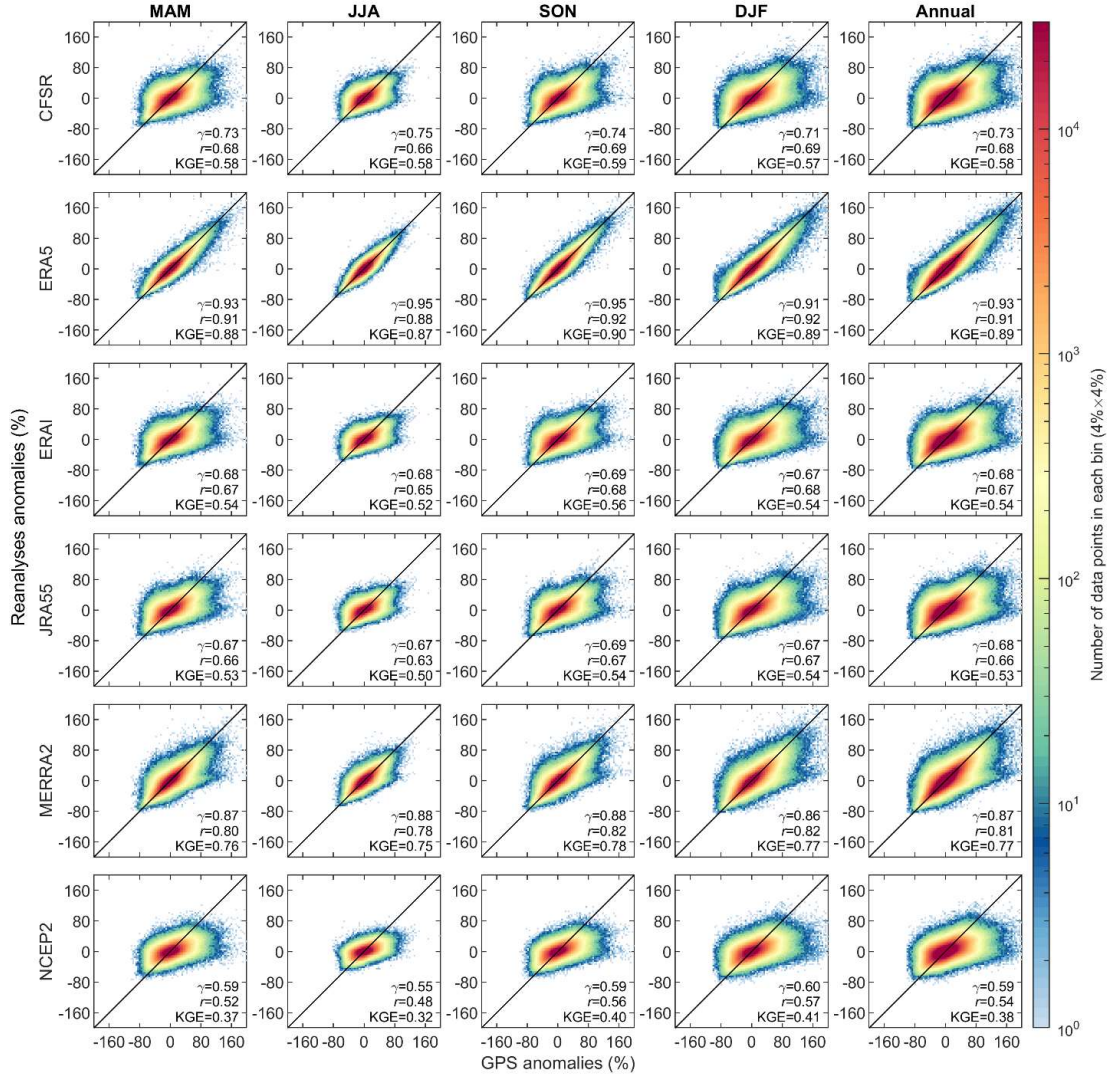

755 **Figure 9.** Scatter plot of the hourly relative anomalies from the daily mean IWV in percentage for the 108 GPS stations. The KGE parameters of the intercomparison are also given.

https://doi.org/10.5194/acp-2021-797
Preprint. Discussion started: 26 October 2021

Atmospheric Chemistry and Physics Discussions

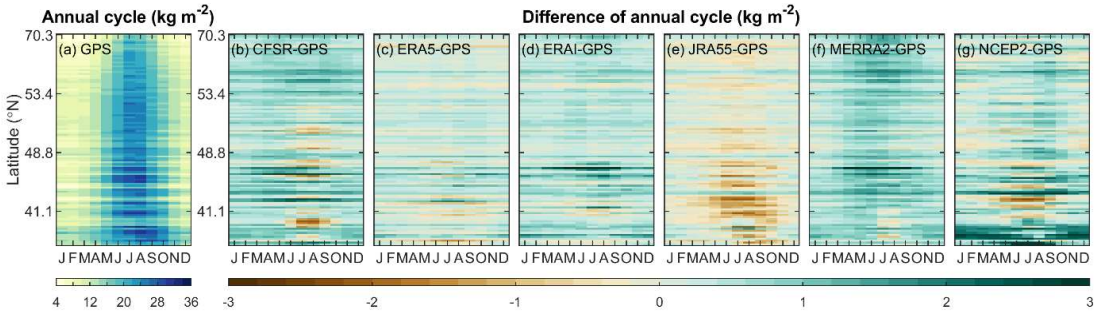

Figure 10. (a) Monthly annual cycle of GPS IWV for the 108 GPS stations. The stations are shown with descending latitudes. (b-g) are the differences of annual cycle from the various reanalyses compared to the GPS.

760

https://doi.org/10.5194/acp-2021-797
Preprint. Discussion started: 26 October 2021

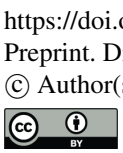

Atmospheric Chemistry and Physics Discussions

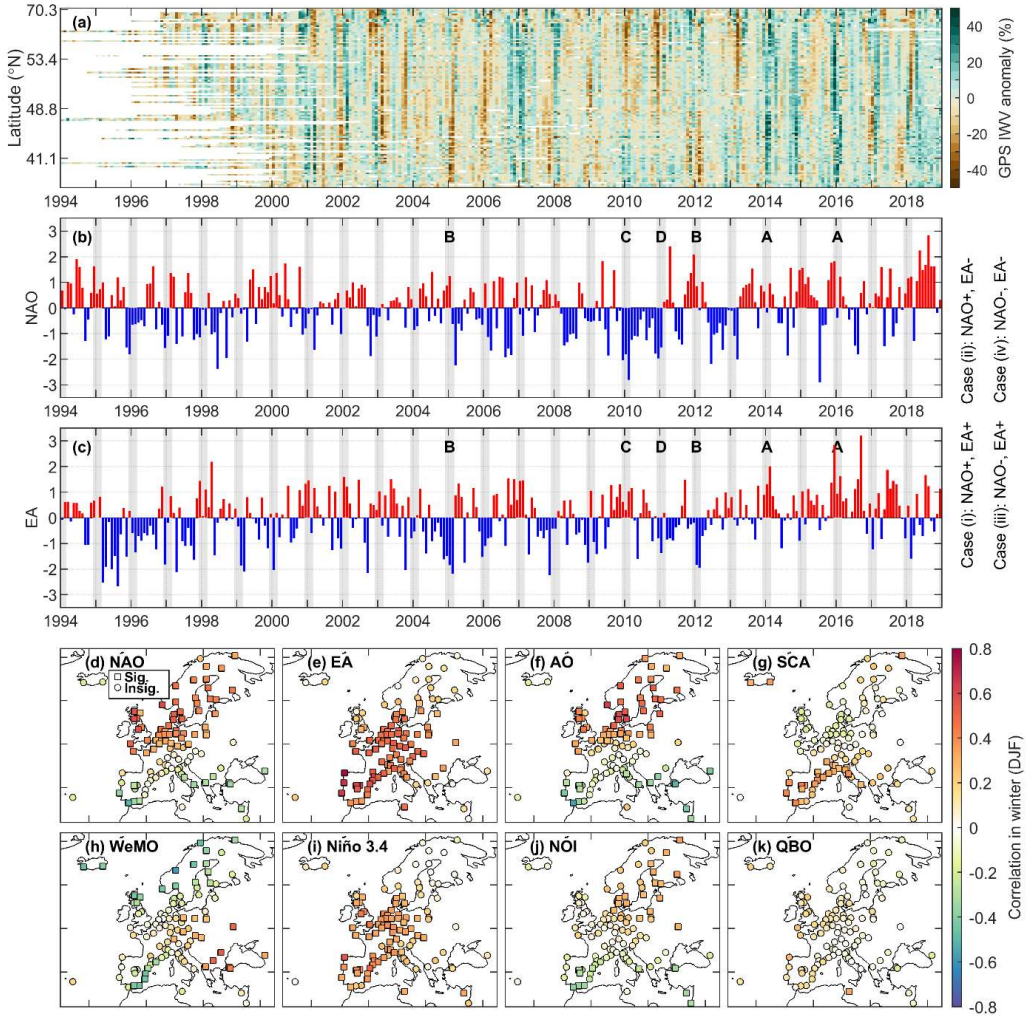

Figure 11. (a) Monthly relative anomalies of GPS IWV for the 108 GPS stations with descending latitudes. (b) and (c) are monthly NAO and EA indices, respectively. The gray bars in (b) and (c) indicates the winter months, i.e., DJF. The winters typically characterized with the four cases (i, ii, iii, and iv) are labelled. (d-k) Spatial correlations between the GPS IWV anomaly time series in the winter months and different teleconnection indices, including NAO (d), EA (e), AO (f), SCA (g), WeMO (h), Niño 3.4 (i), NOI (j), and QBO (k). The squares and circles in (d-k) indicate the Pearson correlation coefficients being significant and insignificant at 95% confidence level using the Student's *t* test, respectively.

https://doi.org/10.5194/acp-2021-797
Preprint. Discussion started: 26 October 2021

Atmospheric Chemistry and Physics Discussions

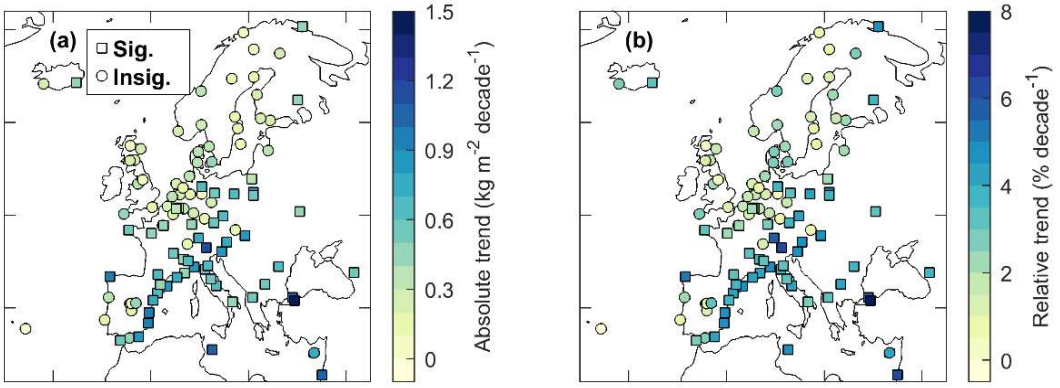

Figure 12. Maps for the absolute (a) and relative (b) trends of the monthly IWV anomaly time series. The relative trend of each station was calculated as the absolute trends divided by the associated average IWV. The squares and circles indicate the trend estimates being significant and insignificant at 95% confidence level, respectively.

https://doi.org/10.5194/acp-2021-797
Preprint. Discussion started: 26 October 2021

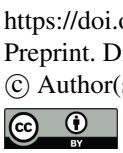

Atmospheric Chemistry and Physics Discussions

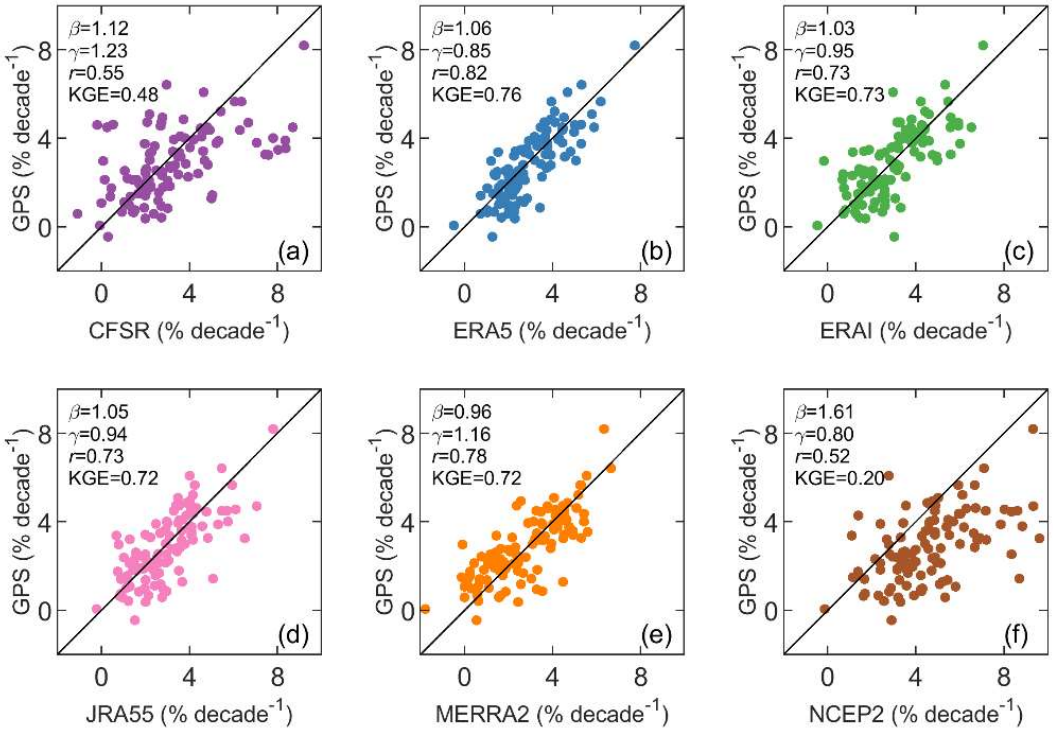

Figure 13. Comparison of the relative IWV trends (% decade^{-1}) from various reanalyses against GPS, respectively.

775

https://doi.org/10.5194/acp-2021-797
Preprint. Discussion started: 26 October 2021

Atmospheric Chemistry and Physics Discussions

Table 1. Six atmospheric reanalyses used in this study and their characteristics.

Reanalysis	CFSR	ERA5	ERAI	JRA55	MERRA2	NCEP2
Source	NCEP	ECMWF	ECMWF	JMA	GMAO	NCEP
Assimilation	3DVAR	4DVAR	4DVAR	4DVAR	3DVAR	3DVAR
Time range	1979-present	1979-present	1979-Aug. 2019	1958-present	1980-present	1979-present
Temporal res. (hour)	6	1	6	6	3	6
Horizontal res. (lat.×lon.)	0.5°×0.5°	0.25°×0.25°	0.75°×0.75°	1.25°×1.25°	0.5°×0.625°	2.5°×2.5°
Pressure levels	37	37	37	37	42	17
References	Saha et al., 2010, 2014	Hersbach et al., 2020	Dee et al., 2011	Kobayashi et al., 2015	Gelaro et al., 2017	Kanamitsu et al., 2002